A Study on Electrical Signal Transmission in Biological Neural Network: Modeling of Gap Junction

By

Hu Xiao Ling

A Thesis

submitted in partial fulfillment of the requirements

for the Degree of

Master of Philosophy

Division of Electronic Engineering

The Chinese University of Hong Kong

Hong Kong, China

June 1999

To my dearest parents.

Acknowledgements

I would like to express my deepest gratitude to my supervisor Prof. Y. T. Zhang for his kind support and guidance throughout the one and half years. Without his help this work could not have been possible. My special thanks to Prof. J. L. Bao, my secondary supervisor in Dept. of BME, Zhejiang University, for introducing me to the exciting world of Biomedical Engineering.

I would also like to express my appreciation to my colleagues in BME lab for making me feel at home. Special thanks to Mr. S. W. Leung, whose help always been a source of inspirations to me. May God bless him. Warmest thanks to Mr. Chu, Mr. L. Y. Xu, Mr. J. Kong, Ms. J. Yao and Miss. K. L. Shuet for making me feel staying at home in Hong Kong. I am grateful to Teacher Hu and Betty for their encouragement and prayers.

My special thanks to my brother and sister-in-law for their never-ceasing encouragement and support, throughout the good and the bad times. Finally, I would like to express my love to my dearest parents, for giving me the chance to experience the life and all encouragement they provided me in all my years spent on educational pursuits.

Abstract

The peak delay, peak attenuation and the increased duration of the post-potential observed at the crayfish's giant motor synapse (GMS), or the rectifying gap junction, were first reported in Furshpan's work in 1959. Based on the understanding of the mechanism at gap junctions and the rectifying hypothesis brought out in Furshpan's report, several models were developed for simulating the behaviors at gap junctions. However, there is no such a model that can more precisely describe the whole properties observed in the experiment at the same time, especially the increased duration at the post-potential.

In this thesis, a new circuitry model is developed for better understanding of the mechanism at the rectifying electrical synapse of GMS. By this new model, the peak delay, peak attenuation and the increased duration can be successfully reconstructed. After the simulation study on the new circuitry model, a theoretical analysis on each junctional elements in the model is carried out, and the results suggest that the junctional capacitance is the major reason for the increased time constant, which affects the peak delay and the duration change at the post-potential of the gap junction. It can provide the useful information in understanding the duration dispersion in some pathological cases. In our work, the new circuitry model is also compared with the most recent kinetic model developed by Giaume for the same rectifying electrical synapse. It shows that

the voltage dependent conductance obtained by Giaume's model can be reconstructed by the model in our work by suitablely adjusting the value of junctional parameters.

As an important mechanism of the excitable membrane, the study on the refractory period of the post-synaptic membrane is carried out as the second part of this thesis when it is inconsistent with that of the pre-membrane. The effects of the absolute refractory period at the post-membrane on the action potential train transmission through the gap junction is studied in our work. Employing the concepts of Point process, the relationship between the absolute refractoriness and the p.d.f. of the output action potential train is concluded by the close-form expression when given the input action potential train is a Poisson process. It is more accurate than the direct truncated Poisson distribution that generally used in neuron firing pattern simulations. The computer simulation work has been done to study the effects from the junctional elements in the model on the action potential train transmission and the effects of the refractory period of the post-membrane on the action potential train transmission when the input is Gaussian distributed interpulse intervals which are commonly detected in the real physiological cases. The results of the simulation show the model elements will greatly affect the average frequency of the output action potential train, and the refractory period of the post-membrane also has the influence on the output firing statistics when given different input firing patterns. The study on the effect of refractory should provide useful information for the design of the electrical stimulators which are widely used in the field of rehabilitation engineering.

论文摘要

在 1959 年,Furshpan 等人在小龙虾巨运动神经突触(GMS)或称整流缝隙连接处记录到了突触后膜动作电位的峰值时延,峰值衰减和电位过程延长. 基于对缝隙连接生理机制的了解和 Furshpan 提出的"整流假说",人们已建立了多个模型用于缝隙连接的仿真.但是这些模型并不能完整地再现实验记录,尤其是突触后膜的时值延长.

在此论文中,我们建立了一个新的电路模型用于更准确地理解 GMS 的信号传递机制,并用此模型重塑了在实验中观察到的后膜动作电位的峰值时延,峰值衰减和电位过程延长.在完成模型的仿真研究后,我们对此新建模型做了理论分析,结果表明, 由于突触电容引入的突触时间常数的增加是导制峰值时延和电位过程延长的主要原因.这一发现可用于解释一些由于突触后动作电位变化引起的病理现象.我们同时将此模型和 Giaume 为稳态时的 GMS 所建立的动力学模型做了比较. 结果表明在表述 GMS 稳态情况下,两个模型结果一致.

作为可兴奋细胞膜的一个特性,不应期在动作电位发放序列传递中的作用成为这一论文的另一内容.应用点过程的分析手段,我们从理论上推出了突触后膜上采集到的动作电位相邻时间间隔的概率密度函数和后膜绝对不应期的数学闭式解.这一结果大大提高了以往人们用直接的截断泊松分布来描述绝对不应期的准确度.在做了理论分析后,我们又做了计算机仿真来研究当输入脉冲序列的时间间隔是高斯分布时的情况,仿真结果显示,不应期和模型参数对于输出动作电位序列的统计特性都会产生一定的影响.

Contents

1 Introduction **1**

1.1 Basic Physiology of the Nervous System 1

1.1.1 Membrane Potential and Its Propagation 2

1.1.2 Cellular Communication 3

1.2 Background of Neural Modeling 5

1.2.1 Models for Membrane 5

1.2.2 The Models for Gap Junctions 9

1.2.3 A Study on the Pulse Train 11

1.3 Main Purposes of the Study 14

1.4 Organization of Thesis 15

2 Electrical Synaptic Model **17**

2.1 Introduction 17

2.2 Model Description 19

2.2.1 An Introduction of the Active Membrane Model 19

2.2.2 The Electrical Synaptic Model 25

2.3 Numerical Calculation 32

2.4 Simulation Results 37

2.5 Discussion 44

3 Analysis of the Synaptic Model **46**

3.1 Introduction 46

3.2 Time Constant Analysis 48

3.2.1 Junctional Time Constant in Bennette's Model 48

3.2.2 The Junctional Time Constant in Our Model 52

3.3 Model Reconstruction 57

3.4 Discussion 62

4 Action Potential Train Transmission Analysis **69**

4.1 Theoretical Analysis on the Refractory Period at the Post-membrane 70

4.1.1 Introduction of Membrane Threshold and Refractory Period 71

4.1.2 Stochastic Models of Neuron Firing 73

4.1.3 Effect of Refractory Period on the p.d.f. of Poisson Process. 78

4.2 Simulation of the Action Potential Train Transmission 85

4.2.1 Effects of the Model Parameter on the Action Potential Train Transmission 90

4.2.2 Effects of the Refractory Period of the Post-membrane on the Action Potential Train Transmission 94

4.3 Results 96

4.3.1 Section Summary 98

5 Conclusions and Future Studies **99**

5.1 Conclusions of Major Contributions 99

5.2 Topics for Future Studies 101

List of Figures

1.1 An action potential recorded at the axon of a squid. 3

1.2 A schematic diagram of the cable model. 6

1.3 Action potential train recorded extracellularly. 12

1.4 The bursts of neuron. 12

2.1 Chord-conductance model(mixed equivalent circuit) employed by Hodgkin and Huxley in their analysis of the squid giant axon, where G_{Na}, G_K and G_L are ionic conductances for sodium, potassium and the combined other small pieces of ions; V_{Na}, V_k and V_L are the equivalent potentials for each ionic channel at the resting potential; C_m is the membrane capacitance. 21

2.2 The model of the rectifying electrical synapse 25

2.3 Ultrastructure of gap junctions at a septum between crayfish lateral giant axons. 27

2.4 Gap junctions. Pores spanning two cell membranes are made of connexin proteins. 28

2.5 Double-voltage-clamp records and corresponding I-V curves demonstrating the peripherally directed current rectification of a perfused motor junction situated between a medial and a motor giant axon. 29

2.6 A schematic diagram of three neighbored channels of the gap junction. 30
2.7 The "all-or-none" property of the F-H block given square current wave with magnitude $1000\mu A/cm^2$ and duration $0.1ms$ as its stimulation. 36
2.8 The calculated curves for pre- and post-membrane. The solid curve is for pre-membrane with the standard stimulation; the other two are obtained at the post-membrane with the fixed value of R_j=$50\Omega \cdot cm^2$ while varied capacitance of C_j, the dotted line with C_j=$10\mu F/cm^2$ and the dashed line with C_j=$20muF/cm^2$. 37
2.9 The calculated curves for pre- and post-membrane. The solid curve is for pre-membrane with the standard stimulation; the other two are obtained at the post-membrane with the fixed value of C_j=$2\mu F/cm^2$ while varied resistance of R_j, the dotted line with R_j=$180\Omega \cdot cm^2$ and the dashed line with R_j=$200\Omega \cdot cm^2$. 38
2.10 The calculated curves for pre- and post-membrane. The solid curve is for pre-membrane with the standard stimulation; the other two are obtained at the post-membrane without taking into account of the value of C_j, the dashed line with R_j=$180\Omega \cdot cm^2$ and the dotted line with R_j=$200\Omega \cdot cm^2$. 38
2.11 The experimental records at the GMS of crayfish. 39
2.12 The attenuation and the peak delay with the change of R_j. The dashed lines are the curves of the peak time delay T_d between the post-potential and the pre-potential; and the solid lines are the curves of peak attenuation V_{at} of the post-potential with respect to the pre-potential. 42

2.13 The attenuation and the peak delay with the change of C_j. The dashed lines are the curves of the peak time delay T_d between the post-potential and the pre-potential; and the solid lines are the curves of peak attenuation V_{at} of the post-potential with respect to the pre-potential. 43

3.1 The model for an electrotonic junction in Bennett' work. The pre-membrane and the post-membrane are only assumed inactive and represented by the passive membrane model. 48

3.2 Postjunctional potential, V_2, obtained by Bennette's model without considering C_c. 50

3.3 The diphasic postjunctional potential, V_2, obtained by Bennette's model when the junctional capacity, C_c, is not negligible. 51

3.4 The simplified circuit with post-membrane only having passive characteristics. 52

3.5 The variation of the post-potential duration with different values of C_j. The three curves in the figure are calculated with $C_j = 2, 10, 15\mu F/cm^2$ given $R_j = 60\Omega.cm^2$ 54

3.6 The variation of the post-potential duration with different values of R_j. The three curves in the figure are calculated with $R_j = 60, 100, 200\Omega.cm^2$ given $C_j = 2\mu F/cm^2$. 55

3.7 Normal histological findings of the right ventricle of control hamster(11 months old) Haematoxylon-eosin; magnification 50x. . . . 56

3.8 Top-Histopathology or the right ventricle of cardiomyopathic hamster(11 months old) showing extensive interstitial fibrosis with Masson trichrome. Magnification 50x. Bottom-Von Kossa's stain of the left ventricle of cardiomyopathic hamster (11 months old) showing central lesion with Ca depots. 58

3.9 Junctional conductances calculated with different parameter setting reported in Giaume's work in 1987[34]. 60

3.10 The comparison between the voltage-dependent conductance calculated using the Boltzmann function and the new circuit model. The dashed line is the result by the Boltzmann function with $V_0 = 40mV$ and $A = 0.13mV^{-1}$; and the solid line is the result by the circuit model with $V_0 = 20mV$ and $V_T = 8mV$, the area of gap junction is $10^{-4}cm^2$ in the calculation. 62

3.11 Junctional rectification demonstrated with voltage steps from resting potential. Inset, V_1 and V_2 were held at the indicated potentials and I_1 was recorded for voltage pulses of about $750ms$ long applied in V_2. The junctional current I_j was measured at the end of each step. Graph, plot of I_j versus the transjunctional voltage $V_j = V_1 - V_2$. 63

3.12 The I-V relationship reconstructed by our circuitry model, when selecting $V_0 = 10mV$, $V_T = 5mV$ and the area of gap junction is $10^{-4}cm^2$. 63

3.13 a. The threshold shifting in Giaume's model, when $V_0 = 10, 20, 30mV$ given $A = 0.5mV^{-1}$. b. The threshold shifting reconstructed by out model, when $V_0 = 10, 20, 30mV$ given $V_T = 5mV$. 65

3.14 a. The adjustment of the sensitivity by Giaume's model, when $A = 0.1, 0.3, 0.6, 0.8mV^{-1}$ given $V_0 = 30mv$. b. The adjustment of the sensitivity reconstructed by our model, when $V_T = 2, 4, 6, 10mV$ given $V_0 = 20mV$. 66

3.15 The I-V relationship at the transjunctional conductance in Giaume's model give $A = 1mV^{-1}$ and $V_0 = 0mV$. 68

4.1 Active responses to small and large depolarizing stimuli. Although the above-threshold stimuli will cause action potentials, the latency will change according to the strength of the stimulus that applied. 71

4.2 The threshold is not fixed. For a short period of time after the firing of an action potential, the threshold is much greater than normal. 72

4.3 Events train 75

4.4 The theoretical calculation results of the p.d.f, $p(\tau)$, when $\lambda_0 = 20pps$ and the absolute refractory period of the post-membrane,μ, is equal to $0ms$ and $20ms$. 83

4.5 Comparison between the theoretical probabilities, the solid lines, and the statistical probabilities, the circles, of simulation of the output IPIs, given $\mu = 5, 10, 15ms$ respectively. 84

4.6 First-order interval histograms for several common processes. a. Pacemaker process; b. Noisy pacemaker process; c. Poisson process; d. Truncated Poisson process; e. Gamma process (r=2,a=25). 87

4.7 Two typical input action potential trains with (a) Poisson distributed IPI when $\lambda = 30pps$ and (b) Gaussian distributed IPI when $\mu = 30ms$ and $\sigma^2 = 50ms^2$. 88

4.8 The histogram of Poisson distributed IPI. 89

4.9 The histogram of Gaussian distributed IPI. 89

4.10 a) The single action potential of the post-membrane with C_j equal to $2\mu F/cm^2$ in the time domain; b) The PDS of the single action potential; c) The action potential train with the variance equal to $1ms^2$ obtained at the post-membrane; d) The PDS of the action potential train. 92

4.11 The pulse train in time domain and its PDS with σ^2 equal to 50 ms^2 and C_j equal to $2\mu F/cm^2$, the mean firing rate λ at 24.5pps. 93

4.12 The relationship between the average frequency $\bar{f}$ and variance σ^2, given C_j equal to $2\mu F/cm^2$ and mean firing rate λ at 24.5pps. . . 93

4.13 The relationship between the variance σ^2 of IPI and $E[S_y(\lambda)/S_y(0)]$, given C_j equal to $2\mu F/cm^2$ and mean firing rate λ at 24.5pps. . . 94

4.14 The relationship between the average frequency $\bar{f}$ and C_j, given variance σ^2 equal to $1ms^2$ and mean firing rate λ at 24.5pps. . . . 94

4.15 (a)The simulated input action potential train generated at the pre-membrane, and (b)the simulation result of the output action potential train obtained at the post-membrane, with the exponential input IPI distribution and the refractory period $\mu = 10ms$. 96

4.16 The relationship between the output mean firing rate and the absolute refractory period for the input exponential IPI distribution with $\lambda_0 = 20pps$. 97

4.17 The relationship between the output mean firing rate and the absolute refractory period for the Gaussian input IPI distribution with $\mu_\tau = 50ms$ and $\sigma = 10ms$. 97

Chapter 1

Introduction

This chapter presents the background information on the electrical physiology of the membrane potential and the way of information transmission in the nervous system. This is followed by an overview of the major achievements of this work, which include the development and analysis of a rectifying electrical synapse model and the study on the action potential train transmission through the model. The purpose of the study is also given. Finally, in the last section of this chapter the overall organization of this thesis is outlined.

1.1 Basic Physiology of the Nervous System

When Dubois Reymond made the first successful laboratory measurements of the nerve impulse in the mid 19th century, he wrote: "If I do not greatly deceive myself, I have succeeded in realizing in full actuality... the hundred years' dream of physicists and physiologists, to wit, the identification of the nervous principle with electricity." In the centuries later on, the understanding of the electrical physiology of neurons, the modeling and the processing of electrical signals in the nervous system have long held a particular fascination for students

and researchers.

1.1.1 Membrane Potential and Its Propagation

Neurons, like all other cells, exhibit a voltage difference known as the membrane potential across their plasma membranes. The membrane potential arises because the plasma membrane is differentially permeable to different ions. When the axon is at rest, that is, when it is not conducting nerve impulses, the value of the membrane potentials called the resting potential. In neurons the resting potential is usually in the range -40 to $-90mV$[1]. By convention membrane potentials are expressed relative to the extracellular fluid, that is, negative membrane potentials indicate that the inside of the cell membrane is more negative than the outside. When the membrane potential is less negative, may be caused by the stimulus from the outside,than the resting potential the cell is depolarized; when it is more negative, the cell is hyperpolarized.

As the depolarizing stimulus gets larger, a critical stimulus strength or threshold is reached, below which only a passive response is seen, and above which a large change in membrane potential several milliseconds in duration may be observed, named the action potential or nerve impulse as shown is Fig. 1.1. It is the signal that responsible for transfer of information from one part of a neuron to another. The actual level of the threshold will vary from neuron to neuron, but it tends to be in the range $10 - 20mV$ depolarized from V_r, the resting potential[2]. Another important property of action potentials is that they are all-or-none events; this all-or-none law, as it is called, is an essential feature of axonal signal transmission, which demonstrates that any stimulus large enough to produce an action potential produces the same size action potential, regardless of stimulus strength.

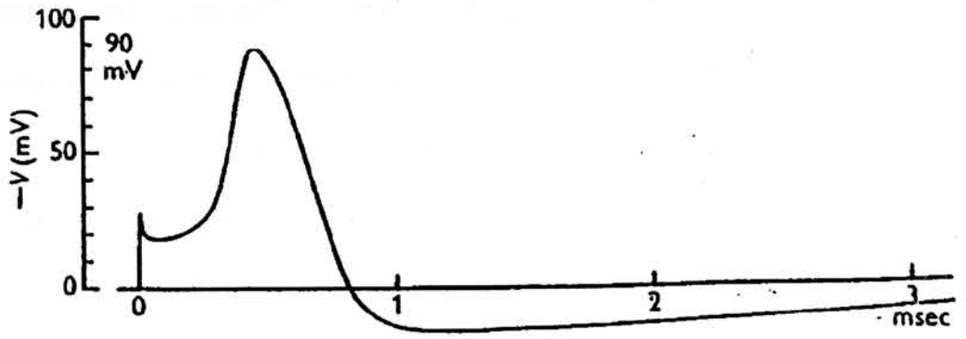

Figure 1.1: An action potential recorded at the axon of a squid[43].

Everything discussed above refers to local changes in the membrane potential at a single point in the axon. However the axon is specialized to move information from one part of the neuron to another. The propagation of the action potential along an axon is realized by the passive spread of the local membrane potential, that is the voltage change does not spread from one point to another, but it is attenuated with distance, until eventually it becomes so small that it is essentially undetectable.

1.1.2 Cellular Communication

Within any organism, cells must be able to communicate. This is of course important in tissues other than the brain, but is essential for proper nervous system function. There are three general ways in which cells talk to each other[61]:

1.Direct transfer of molecules and ions from the cytoplasm of one cell into that of another, such connection is called gap junction.

2.The release of a chemical that diffuses to, and acts on, another cell. This release process is termed secretion.

3.Direct physical contact. A cell can be influenced profoundly by events triggered when molecules in its plasma membrane interact with the membranes of adjacent cells.

In most cases, synapses are chemical ones. When information has to be transferred form one cell to a distant cell, the usual mechanism is for the first cell to release a chemical into the extracellular space. This chemical then either diffuses to, or is transported to, the target cell. These include amino acids and other small organic compounds, lipids, small peptides, and large protein complexes. Chemical that are released from a neuron, and alter the excitability of another neuron or a muscle cell, are termed neurotransmitters[1].

Gap junctions are another kind of synapse which constitute a very basic and rapid form of communication by direct electrical current transmission between neurons. Because of the signal transmission characteristic of gap junctions, it is comparatively easier to describe the function of gap junction by electrical models. It is also the reason for us, electrical engineers, chose gap junction as the object to model in this work.

One of the functions of gap junctions is to allow the transfer between cells of ions involved in intracellular signaling, and of small molecules that are important for development. This in turn, allows a group of cells to act as one functional unit. In the nervous system and other excitable tissues, gap junctions take on a special significance. Connections between nerve cells via gap junctions are often called electrical synapses, in recognition of the fact that they are involved in rapid electrical signaling and information transfer. For example, the electrical synapse at the Giant Motor Synapse (GMS) of a crayfish which participates in the neural circuitry underlying a rapid escape response[51]. Similar electrical synapse is also found at a synapse in the brain of a vertebrate, the hachetfish[5]. In the brain of human beings, there are a lot of electrical synapse which are important while we wiring up the brain.

Gap junctions are abundant not only in the nervous system but also in tissues such as the liver, the lens and the heart. Because of its important role in normal cell function, the disruption of gap junction communication may lead to disease processes. For example, micro-reentry arrhythmias are a major cause of sudden death in patients with coronary heart disease[6][7] [8][9][10]. Although alterations in the active ionic membrane properties of the myocyte may contribute to the genesis of these arrhythmias, abnormal intercellular conduction appears, in many instances, to be the key underlying factor[11].Thus study on gap junction is necessary not only for the reason that it is one types of structure for cells' communication, but also such study will provide diagnostic importance.

1.2 Background of Neural Modeling

The goal of neural modeling is to relate, in nervous systems, function to structure on the basis of operation. The activities of neural modelers are thus largely concerned with the working out of various characteristics and peculiarities of the operational dynamics of the systems, and cells of nervous tissue. In this light it is easy to see that the orientation of engineering is appropriate for the area, and to understand that modeling work has been performed in large part by engineers. This has been advantageous in that powerful quantitative and analytic techniques have been used and are available in the area.

1.2.1 Models for Membrane

The modeling in the nervous system may be dated back from the models of passive membrane. From the point of view of irreversible thermodynamics, one of the most widely used models of passive membrane is the Nernst-Planck equation,

which simply combines Ohm's law for the flow of charged particles in an electrical potential gradient and Fick's first law for the diffusion of particles in a concentration gradient[12]. By the assumption that the membrane is homogeneous and in an isotonic system of ions of one valence, the Nernst-Planck equation may be simplified to the Goldman equation which is commonly used to estimate the resting potential of the biological membrane[13].

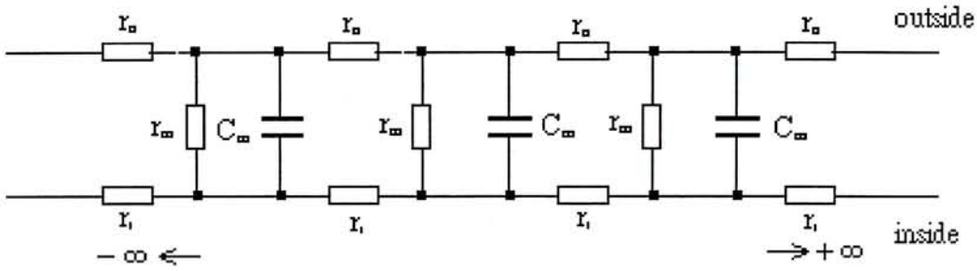

Figure 1.2: A schematic diagram of the cable model.

Different from the Nernst-Planck equation who is based on the point of view of membrane physics, some circuit models are probably more convenient and revealing to illustrate the signal flow over distributed neuronal structures. The membrane of a nerve cell, or indeed of any cell, provides an extremely thin insulating layer between two conducting solutions. This allows the membrane to separate and store charge, and thus it is also an electrical capacitor with some membrane capacitance. Based on this idea, a cable model as shown in Fig. 1.2 was proposed to analyze the passive spread alone a nerve fiber[14]. The change of the voltage across the membrane and its transmission along the fiber can be described by Equ. 1.1,

$$-\lambda^2 \frac{\partial^2 V_m}{\partial x^2} + \tau \frac{\partial V_m}{\partial t} + V_m = 0, \tag{1.1}$$

where λ is the space constant, τ is the time constant and V_m is the cross-membrane voltage. If given

the boundary condition of the equation as:

$V_m = 0$ $(x = \pm\infty)$,

the initial condition as

$V_m = 0$ $(-\infty < t < 0)$

and

$I = I_0$ $(t = 0)$,

then the analytic solution of the equation will be

$$V_m(X,T) = \frac{r_1 I_0 \lambda}{4}\{e^{-|X|}[1 - erf(\frac{|X|}{2\sqrt{T}} - \sqrt{T})] - e^{|X|}[1 - erf(\frac{|X|}{2\sqrt{T}} + \sqrt{T})]\} \quad (1.2)$$

where $X = x/\lambda$ and $T = t/\tau$.

From Equ. 1.2, it suggests that the passive conducted signals are attenuated almost exponentially with the distances x. When such signals are excitatory, they may lead to the generation of large-amplitude spikes, which in turn are continually provided with energy as they propagate and thus are conducted over essentially unlimited distances without attenuation. Based on observed, dynamic changes in chord conductances of the membrane of the squid giant axon, Hodgkin and Huxley built up an active membrane model, named H-H, to account for the changes prior to, during, and following an action potential in 1959. It is because of the model that Hodgkin and Huxley won the Nobel Prize. By modification on the H-H model, it also may be used to account for the action potentials of some other types of cells. For example, in 1964, Frankenhaeuser and Huxley developed an F-H model to illustrate the behavior observed in the myelinated nerve fiber of the Xenopus laevis. F-H model is similar to H-H, the major difference is there is a 'non-specific current' in F-H which is mainly induced by the current of sodium but possibly also by other ions such as calcium[15].

H-H model marks the beginning of the quantitative modeling of the active membrane. Based on this prototype, not only F-H model but also many other

models are developed to illustrate the mechanism of some specific cell membranes, for example in the cardiac system. The cardiac action potential is more complex and the associated ionic currents are more numerous than that of the giant squid axon used for H-H. The action potential in heart cells shows a rapid depolarization phase, then a plateau in which the cross membrane voltage, V_m, changes very slowly and which lasts for 100 to $200ms$, and finally a repolarization phase that is slower than in the axon. A fast inward current (mainly carried by Na^+ ions) causes the depolarization phase, while repolarization is due to a net outward (mainly K^+) current. During the plateau phase, which is absent in the action potential of axons, V_m changes very slowly due to a delicate balance between inward and outward currents. It is now known that the inward current during the plateau is mainly carried by Ca^{2+} ions, while the outward currents correspond to different families of K^+ channels.

In the first attempts to model the action potential of cardiac cells, researchers tried to modify the original H-H equations to account for the main features of cardiac potentials. In 1962, Noble adapted the H-H model to simulate the action potential of purkinje fiber[16]. He modified the kinetics of the inward I_{Na} to account for the plateau phase and divided I_k into two components (I_{K1} and I_{K2}), I_{K2} was formally similar to the H-H model's K^+ current, while I_{K2} was responsible for the spontaneous pacemaker activity of Purkinje cells.

In 1975, after the discovery of many new currents, McAllister, Noble, and Wesien improved Noble's model by including a secondary inward current (I_{si}, carried by Na^+ and Ca^{2+} ions) which supported the plateau of the action potential , and further divided the K^+ current into three distinct components[17]. It was not until 1985 that a very detailed model of the Purkinje fiber action potential appeared: the DiFrancesco-Noble (DN) model[18].

Parallel to the development of Purkinje fiber models, the action potential of ventricular myocytes was also simulated. in 1977, Beeler and Reuter (BR) formulated a set of equations that reproduced the ventricular action potential[19]. The BR model, which was modified by Drouhard and Roberge in 1982[20], was used until the Luo and Rudy (LR) models are formulated in the present decade[21][22]. The LR model is being updated and improved by several research groups by including new ionic currents[23][24]. At the same time, other models of the ventricular action potential[25] as well as models of other types of cells have appeared[26][27].

In this work F-H model is used, the first reason is for the simplicity and the other is because what we studied is the function of the gap junction, connection between cells, but not mainly the membrane.

1.2.2 The Models for Gap Junctions

The experimental observations on the transmission at the Giant Motor synapse of the crayfish was first reported by Furshpan and Potter in 1959[28]. In that report, it indicates that the junction operates by means of "electrical", transmission, and it behaves like an electrical rectifier. Based on the "rectifying hypothesis" in that paper some models are developed in the following decades.

It is believed that the open and the close of the channels at the electrical synapse mainly affects the resistance at the gap junction. The most simplest model for an electrically coupled synapse is only a pure resistor, if not rectifying, or a diode, if rectifying, as for the GMS of the crayfish. The resistor-represented gap junction is widely employed in many gap junction related studies, like Cole's work on gap junction uncoupling and discontinuous propagation in the heart in 1988[42],Cartee and Plonsey's work on the transient subthreshold response of a

one-dimensional cardiac model in 1992[30], Thakor's report on the modeling of two-dimensional cell network of heart, CELLSIM, in 1998[31], and et al.. Comparing to the development in the modeling of the membrane, progress made in modeling of gap junction is not very great. In electrical circuit models, the widely accepted is the resistor model mentioned above, while there once was a model developed by Bennett who added a capacitor in parallel with the original junctional resistor in 1966[32]. However finally it is reported in that paper this parallel connected capacitor may be ignored. In 1998, there is a similar gap junction circuit model brought out in Fear and Stuchly's study on biological cells with gap junctions in low-frequency electric fields, while the same conclusion that the parallel connected junctional capacitor may be ignored in low-frequency field is also reached[33].

A more finely developed kinetic model for the rectifying electrical synapse of the crayfish is the one proposed by Giaume and et al. in 1987[34]. In fact it is also resistive but forward biased, like a diode. In that model the junctional resistance of the rectifying synapse was modeled by a simplified Boltzmann function according to the regression over the experimental data of voltage-clamp. The Boltzmann function basicly displays the voltage-dependent characteristics of the synapse.

It seems that the pure resistive gap junction model is enough to describe the whole picture of the gap junction. However, there is some difficulty for both the simplified Boltzmann function and the resistor circuit model to reconstruct some transient behaviors such as the delay, the peak attenuation of the action potentials at the post-membrane observed in Potter's experiment.

In this work, a new circuitry model was proposed with the intention to understand the mechanism of the rectifying electrical synapse from another angle

and one step further, especially on the dynamic factors that cause the peak delay and peak attenuation that observed in the experiments.

After the development of the circuitry model, a comparison also was made between Giaume's model and the circuitry model, it is found that the new model not only possesses the properties owned by Giaume's model but also may be used to illustrate the transient behaviors not in Giaume's work. By theoretically analyzing the new circuitry model, it suggests that the time constant at the synapse plays a very important role in controlling the peak attenuation, peak delay and the duration change that may be observed in some pathological cases.

1.2.3 A Study on the Pulse Train

Although the generation of an action potential is fundamental to a neuron's ability to transmit information, there are many other aspects of its electrical properties that play important roles in shaping neuronal or synaptic input and output. Some neurons have a steady unchanging resting potential in the absence of external stimulation, that is, they are silent. Other neurons, However, generate a variety of endogenous electrical patterns. For example, Some neurons may beat, that is they fire repetitively at constant frequency. Some cells fire spontaneously in the absence of external stimulation and do not fire at fixed regular intervals as shown in Fig. 1.3. Some neurons do not fire spontaneously but instead generate regular bursts of action potentials as shown in Fig. 1.4. Such cells are termed bursting neurons. This ability of a neuron to burst repetitively is used by the nervous system in at least two different ways:

- Bursting neurons generate rhythmic behaviors, although the intervals between action potentials in a burst are usually irregular. Many fundamental behaviors, such as breathing, walking, swimming, and the chewing of food,

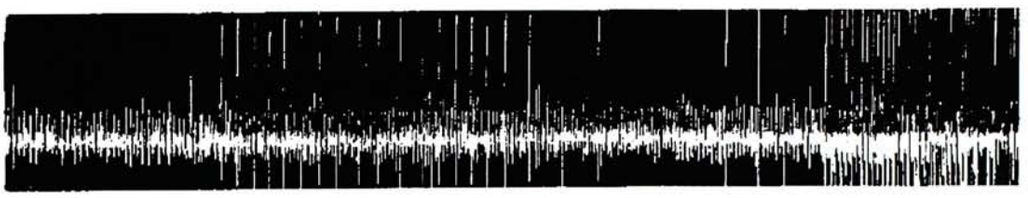

Figure 1.3: Action potential train recorded extracellularly.

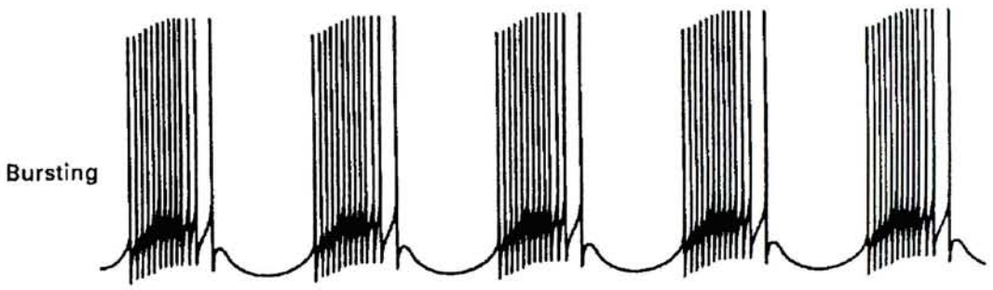

Figure 1.4: The bursts of neuron.

require the continual rhythmic stimulation of a group of muscles. Numerous examples of electrical bursting can be found in neuronal circuits that generate such rhythmic motor outputs. Although in many cases the exact form and timing of the bursts, and even their generation, may be regulated by interactions among several different neurons, the ability to generate bursts can also be intrinsic to specific neurons that continue to burst in the absence of external inputs.

- Bursting neurons are used to secrete neurohormones. Neurons, in addition to acting directly on other neurons or on muscle cells, may secrete hormones into the circulation.

From the introduction of the firing patterns of neurons, it is clear that not only single action potentials are the information carriers in the nervous system but also the sequence of an action potential train also may contain biological informations during the transmission. Furthermore, action potential trains with regular interpulse intervals (IPIs) or with random interpulse intervals are the

main appearance of the living signals in the nervous system. Therefore, it will be more meaningful to carry out the study on the action potential train transmission through the synapse. In this work, the transmission of the action potential train with various distributions of IPIs through the rectifying electrical synapse was studied. Although the firing patterns chosen in our study are comparatively simpler than those in the real cases, the bursting pattern has not been simulated in this work yet, it is the first step to relate the model built in our work to the signal processing characteristics of nervous system in our work. The idea and its simulation results probably will give some inspiring suggestions to both physicians and engineers who are working in this specific area.

When doing the analysis on the pulse train transmission through the synapse, the refractory period of the synaptic membrane is another factor that affects the performance of the action potential train transmission. The refractory period, especially the absolute refractory period, is a regulation mechanism of the excitable membrane that for several milliseconds after the firing of an action potential, it is impossible to evoke another action potential no matter how large the depolarizing stimulus. Therefore when the interpulse interval of the incoming action potential train is less than the absolute refractory period of the post-membrane then some action potentials in the input will not evoke the corresponding action potentials at the post-membrane. Consequently the distribution of the IPI of the output action potential train obtain at the post-membrane may not be same as that of the input action potential train at the pre-membrane. Several mathematical models have be established to simulate the refractoriness of the membrane when studying the generation of an action potential train. Gray, in 1967, and Gaumond et al, in 1982, described how the neuron recovers its ability to fire after generating an action potential by summarizing the refractoriness as a recovery function which

represents the firing ability of membrane recovers from the refractoriness[35][36]. Given a choice of recovery function, the measured spiked train can be used to estimate a free firing rate, namely the firing rate of the neuron when it is not under the influence of refractoriness. This study was carried out by Johnson and swami in 1983, and Miller in 1985[37][38]. The most recent work on the effect of the absolute refractory period on the action potential train is reported by Berry and Meister in 1998 in the study of retinal ganglion cells where a recovery function is also used to simulate the absolute refractory period[39].

In this work, the effects of the refractory period on the action potential train transmission through the electrical synapse are analyzed, with the assumption that the input action potential train is a homogeneous Poisson Process. Different from the refractoriness models, or recovery functions mentioned above, we did not do the study about the generation of the action potential train at the membrane, but focus on how the refractoriness of the post-membrane affects the action potential train which has been generated by the pre-membrane going through the gap junction. Thus the method for modeling the refractory period in this work, which is detailed in Chapter 4, is different from the recovery function introduced above.

1.3 Main Purposes of the Study

The original motivation of this work was triggered by the observation of the defects of the gap junction models in recent researches. We have the idea whether it is possible to improve the model of gap junctions and then to do some further model-related studies. The main purposes of our study are listed as follows:

- To develop a new model which can more precisely describe the transient

behaviors of the gap junction. Since the gap junction models used at present are not capable in depicting some basic properties that observed in the experiment, like the peak delay and the increased duration at the post-potential.

- To do the theoretical analysis on the gap junction model after the development of the model, trying to find a suitable measure to qualify the transient behaviors at the gap junction.

- To compare the new model with the kinetic model developed by Giaume for the same electrical synapse, trying to find the similarities and the differences between the two models.

- To relate the mechanism of the refractory period of the post-membrane to the function of the gap junction model, trying to find the characteristics of the action potential train transmission through the gap junction by theoretical analysis and simulation study.

1.4 Organization of Thesis

This thesis is divided into two major parts. The first part is on the development and theoretical analysis of the rectifying electrical synaptic model. The second part is on the simulation of the action potential train transmission and the analysis on the refractory period.

Chapter 1 provides the background information on some necessary basic physiology of the biological nervous system, the history of modeling in this area, and an overview of the thesis.

Chapter 2 provides the detailed computer simulation methods, results and analysis on the model. In the first part of this chapter, the physiological and

mathematical background of the model are introduced. That follows the description of the computer simulation method, then the results of the simulation are given and analyzed. Finally, a short discussion is provided at the end of the chapter.

Chapter 3 presents the theoretical analysis on the model, based on the simulation results introduced in Chapter 2. The time constant as a key quality which affects the behavior of gap junction is analyzed and also compared with the time constant for another gap junction model introduced by Bennett. The model reconstruction part in this chapter makes the comparison between the model in our work and the model developed in Giaume's work.

Chapter 4 presents the study on the action potential train transmission through the gap junction model. In the first part of this chapter, a theoretical analysis on the effect of the absolute refractory period of the post-membrane on the probability density function of the output action potential train is carried out. The second part of this chapter is the computer simulation of the action potential train transmission through the gap junction model given different IPI distributions in order to investigate the functions of junctional elements on the pulse train transmission.

Chapter 5 concludes the original contributions in this thesis and raise some potential research directions based on the proposed methods.

Chapter 2

Electrical Synaptic Model

2.1 Introduction

The original motivation of the development of the model for the rectifying electrical synapse is trying to provide a better understanding of the mechanism at the GMS of the crayfish. In Furshpan's work, comparing the action potentials detected at the Lateral giant fiber (the pre-membrane) with those at the giant motor fiber (the post-membrane), the changes in the shape of the action potential after the synaptic transmission are obvious[28]. The action potentials at the post-membrane evoked by the impulses from the pre-membrane are less in amplitude, greater in duration and delayed in their peak time. These phenomena may suggest there are some subtle changes, maybe due to the structure of the synapse, during the directly electrical transmission at the gap junction.

Although there are some models proposed to simulate the behaviors of the synapse as mentioned in Chapter 1, almost all of them assume that the electrical synapses only have the pure resistive property. However by these models, the increased duration of the post-potential will not be obtained. Although

it was mentioned in Bennett's work about the physiology of electrotonic junctions that there may exist a capacitance element in parallel with the junctional resistance[32]. While also it was pointed out by Peter A. Getting in 1973 that the capacitance should be negligible otherwise it would not be the peak delay but the peak advance will be detected at the post-membrane[40]. Until now there is no such a specific model which can more accurately describe the characteristics of the gap junction.

To do some further study on the mechanism of gap junctional transmission is necessary. The new circuitry model developed in our work meets the requirement of the more precise reconstruction of the transmission properties at the gap junction of the GMS. Furthermore from the simulation results of our modeling work, it is interesting to find that some results even may be helpful to illustrate some phenomena observed in pathological cases. Some tissues mediated by electrical synapses or gap junctions are always need the uniformed reaction of a large pool of cells in the normal organ. The dispersion of the action potentials at the post-membrane in the shapes may correspond to some diseases, such as the ischemia in the heart or in some tumor processes[41]. Therefore the study on the gap junction model is meaningful not only for the progress will be made in engineering but also for providing some help in diagnosis.

In this chapter, as an essential part of the rectifying electrical synapse model in our work, the active membrane model is introduced in the first part of this chapter. It is followed by the description of the model we developed. Then the numerical calculation method which is used in the simulation is also illustrated as a section in the chapter. In section 2.4, we give the simulation results produced by the model, and also they are compared with the experimental data. Finally, this chapter concludes with a discussion on the simulation of the model.

2.2 Model Description

In this section, the new circuitry model for the rectifying gap junction of crayfish' GMS is introduced. While in the first part of this section, some basic concepts on the active membrane model are given. Since the active membrane model serves as an essential role in our work. That follows the detailed illustration of the gap junction model.

2.2.1 An Introduction of the Active Membrane Model

The best way to begin an introduction of the active membrane model is to choose Hodgkin-Huxley model[43] as the example and the experiments that immediately preceded it. Since H-H model is the most classical one and the active membrane models that appeared later on are all derived from it. Using the voltage-clamp techniques that had been developed by Cole and others[42], Hodgkin and Huxley shifted the membrane potential of the squid giant axon and observed the resulting currents. Because of the large diameter of that axon, they were actually able to thrust a pair of fine, independent silver electrodes through the cut end of the axon and into its axoplasm for a considerable distance. Thus, they were able to effectively short-circuit a segment of axoplasm, making it essentially isopotential over its length. Employing a clever guard system and cylindrical electrodes, they were able to make the adjacent extracellular solution (seawater) isopotential as well, elimination all axial components of current and leaving only the possibility of radial components in the portion of the axon being voltage clamped. Thus, in effect, they were applying the clamp to a fairly large patch of membrane. This technique generally is called the space clamp.

In response to a step wise depolarization of the membrane from its resting potential or some voltage close to the resting potential, they observed four phases

of current. First, there was a very brief current spike, discharging the membrane capacitance and thus allowing the membrane potential to shift to its new level. As soon as this spike subsided (which required only a few microseconds), they observed an increase in the net outward current (just as one would expect in response to a depolarization in a passive-membrane system). Within a fraction of a millisecond, however, this outward current gave way to a net inward current, which, if the membrane were not clamped by a nearly ideal voltage source, would bring about further depolarization. This time course and magnitude of this inward current phase depended markedly on the magnitude of the depolarizing step and on the voltage from which the step was make. Generally, within 1 or 2 msec, the inward phase was overwhelmed by a second outward phase, whose dynamics and magnitude also depended upon the size of the voltage step and the membrane potential prior to it. This outward phase persisted for many tens of milliseconds if the clamped depolarization were maintained, but subsided rather quickly if the membrane were repolarized.

Substitution of chorine ions for the sodium ions of the seawater bath abolished the inward phase of the current. Under these circumstances, the growth of the late outward phase could be observed to begin almost immediately after the clamped-voltage step, being continuous with the early outward phase. Thus, the picture emerged of a single outward phase, interrupted by a transitory inward phase when sodium ions were present in the extracellular solution. The reversal potential for the outward phase was very close to the Nernst potential for potassium ions, while that of the inward current was very close to the Nernst potential for sodium ions. Since the outward current was carried predominantly by potassium ions and the inward current was carried predominantly by sodium ions when the membrane is excited.

To model the system they were observing, Hodgkin and Huxley selected a mixed equivalent circuit with chord conductances and fixed reversal (Nernst) potentials for potassium and sodium ions and a combined chord conductance and fixed reversal potential for all other ions species. They assumed that the combined chord conductance for the other ions was constant and estimated its magnitude on the basis of data from the membrane near its resting state. The membrane capacitance was found to be quite constant over the entire voltage range of interest; so the only variable parameters in their model were the sodium and potassium chord conductances. The assumed potassium and sodium were distinguished experimentally on the basis of the choline experiments, and the corresponding conductance values were found and consistent with the equivalent circuit in Fig. 2.7.

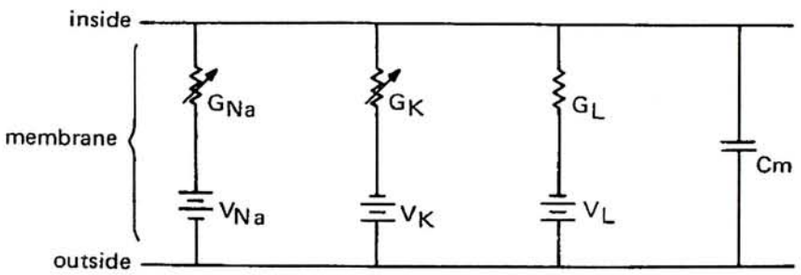

Figure 2.1: Chord-conductance model(mixed equivalent circuit) employed by Hodgkin and Huxley in their analysis of the squid giant axon, where G_{Na}, G_K and G_L are ionic conductances for sodium, potassium and the combined other small pieces of ions; V_{Na}, V_k and V_L are the equivalent potentials for each ionic channel at the resting potential; C_m is the membrane capacitance.

In response to a stepwise depolarization, the potassium chord conductance increased gradually, with a deep inflection, then approached a final magnitude which was maintained. In response to a stepwise repolarization or hyperpolarization, the potassium chord conductance decreased in a noninflected manner toward a final, lower magnitude. The rate at which the potassium chord conductance rose and the final magnitude it attained both increased monotonically as

the amplitude of the stepwise depolarization was increased. In order to describe the dynamics of this chord conductance for their model, Hodgkin and Huxley sought a mathematical function that would exhibit both an inflected rise and a noninflected fall. The function that they selected is

$$f(t) = (a + be^{-ct})^{\beta}, \tag{2.1}$$

where the initial value is $(a + b)^{\beta}$ and the final value is a^{β}. If the final value is greater than the initial value, then b must be negative, and the transition from $a + b$ to a will be inflected. On the other hand, if the final value is less than the initial value, then b must be positive and the transition will be noninflected. Thus, the function of Equ. 2.1 was a reasonable candidate for describing the inflected rise and noninflected fall of the potassium chord conductance. What remained was to select a, b, c, and β to provide the best fit to the data. Noting that the term within the parentheses on the right side of Equ. 2.1 is the solution of a simple linear differential equation, Hodgkin and Huxley described their observed potassium chord conductance as follows:

$$G_K = \bar{g}_K n^4 \tag{2.2}$$

$$\frac{dn}{dt} = \frac{n_{ss} - n}{\tau_n} \tag{2.3}$$

where $\bar{g}_K$ is a constant and n_{ss} and τ depend on membrane potential. All of the voltage dependence of the dynamic chord conductance is thus associated with the two parameters n_{ss} and τ_n, while all of the innate time dependence is embodied in the differential equation. Hodgkin and Huxley used curve-fitting methods to develop equations to describe the dependences of $\tau - n$ and n_{ss} on membrane potential.

In response to a stepwise depolarization, the dynamic chord conductance for

sodium ions rose with an inflection, passed through a peak, then fell again to a low magnitude. If the membrane suddenly were repolarized, the sodium chord conductance fell much more rapidly and in a distinctly noninflected manner. To describe the inflected rise and noninflected, rapid fall of the sodium chord conductance, Hodgkin and Huxley again used the function of Equ. 2.1. To describe the slower fall, which took place when the depolarization was maintained, they used the same basic function, but with β set equal to unity. Again, parameters (τ_m, m_{ss}, τ_h, and h_{ss} which represent the potassium conductance dependence of membrane potential) were found by matching the experimental data, and the conductance dynamics were embodied in linear differential equations:

$$G_{Na} = \bar{g}_{Na} m^3 h \tag{2.4}$$

$$\frac{dm}{dt} = \frac{m_{ss} - m}{\tau_m} \tag{2.5}$$

$$\frac{dh}{dt} = \frac{h_{ss} - h}{\tau_h} \tag{2.6}$$

The dynamic equation for the mixed equivalent circuit employed by Hodgkin and Huxley is simply

$$\frac{dV}{dt} = -\frac{1}{C_m}[G_K(V - V_K) + G_{Na}(V - V_{Na}) + G_L(V - V_L)] \tag{2.7}$$

where V is the membrane potential. By combining Equ. 2.3, Equ. 2.6 and Equ. 2.7, Hodgkin and Huxley had a complete dynamic description of the space-clamped patch of squid-axon membrane, derived under the rather severe constraint of voltage clamp. The next obvious step was to determine whether or not this same set of equations correctly described the dynamics of the unconstrained axon membrane prior to, during, and following a spike. Incorporating an impulse-like depolarizing current in their equations, Hodgkin and Huxley calculated the corresponding responses of the two dynamic chord conductances and the membrane potential and found excellent correspondence with the observations on the

actual axon. In other words, they had, in their equations, an excellent dynamic description of the unconstrained axon as well as the clamped axon. The equations themselves are now known collectively as the Hodgkin-Huxley model.

The model of H-H apparently apply specifically only to the squid giant axon, but with rather minor modifications they appear to be applicable to other invertebrate axons, e.g., see Dalton and FitzHugh, 1960[44], and to myelinated axons in several vertebrates as the F-H equation for toad *Xenopus laevis* by Frankenhaeuser and Huxley which is used in our work[15]. The method for obtaining the F-H model follows that used in completing the H-H equation by curve fitting introduced above. The membrane potential was changed in steps and membrane current was recorded. Equations were then fitted to the results so as to express the component ionic currents as functions of membrane potential and time. The following is the expression of the F-H model.

$$\begin{aligned} I &= I_c + I_i, \\ I_i &= I_{Na} + I_K + I_p + I_L, \end{aligned} \tag{2.8}$$

where I_c is the capacitance current and I_i is ionic current composed by sodium, potassium, leak current same as those in H-H model, and a non-specific current, denoted as I_p, which is the major difference between the H-H model and F-H model. The non-specific current is a part of the complex delayed current carried mainly by potassium[45][46][47]. While I_P itself is to a large extent carried by sodium, but possibly also by other ions such as calcium[48]. Although there are some differences between active membrane models, following a depolarization that exceeds threshold, the general phenomena that those models represent are apparently almost universal in spike-generating nervous tissue.

2.2.2 The Electrical Synaptic Model

The rectifying synaptic model for GMS of the crayfish proposed in our work is composed of two parts as shown in Fig. 2.2. It is composed of two parts, the membrane part and the junctional part.

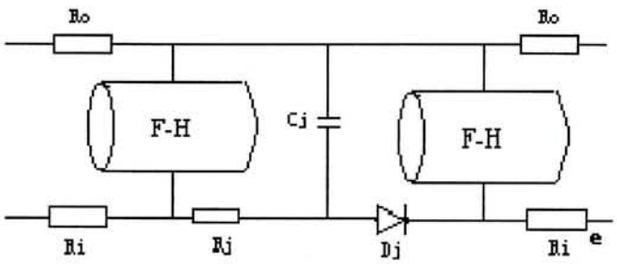

Figure 2.2: The model of the rectifying electrical synapse

The first part is for the pre- and post-membrane modeled by two F-H blocks which can produce action potentials by F-H equation. As introduced in the section of the active membrane model, that the fibers form the GMS are the myelinated ones. It can be seen from Fig. 2.3[49]. It is the reason why the F-H equation was chosen is that it is especially for myelinated nerve fiber, which is the type of the neurons forming the synapse under study. In the membrane modeling, the pre- and the post-membrane have been assumed to be symmetric. Namely, the same set of membrane parameters are used in both pre- and post- F-H blocks.

By the technique of freeze fracture induced by Makowski et al[50]. the channels of the gap junction that couple two neighboring cells together may be visualized as shown in Fig. 2.4. Through the channels that embedded in the pre- and post-membrane, small molecules and ions in one cell diffuse through pores in the plasma membrane directly into the cytoplasm of the neighboring cell. The synaptic part in the model consists of a resistor R_j, a capacitor C_j and an ideal diode D_j. Since the transjunctional current flows directly through the channels of the gap junction, the resistance that ionic current meets there is represented

by a resistor, R_j. The diode D_j is based on the voltage dependent characteristic of the GMS which is first reported as the "rectifying hypothesis" in Potter's work. As we now know, the voltage dependent characteristic is due to the gating mechanism of the gap junction channels which are sensitive to the junctional voltage across them. For the rectifying electrical synapse of the crayfish, it is one-way gating, that is, when the gates at the gap junction will be open only when the cross-junctional voltage is in one direction, otherwise the gates will close. The population reaction of the open or close of the channels at the GMS can be depicted by the I-V relationship given in Fig. 2.5[51].

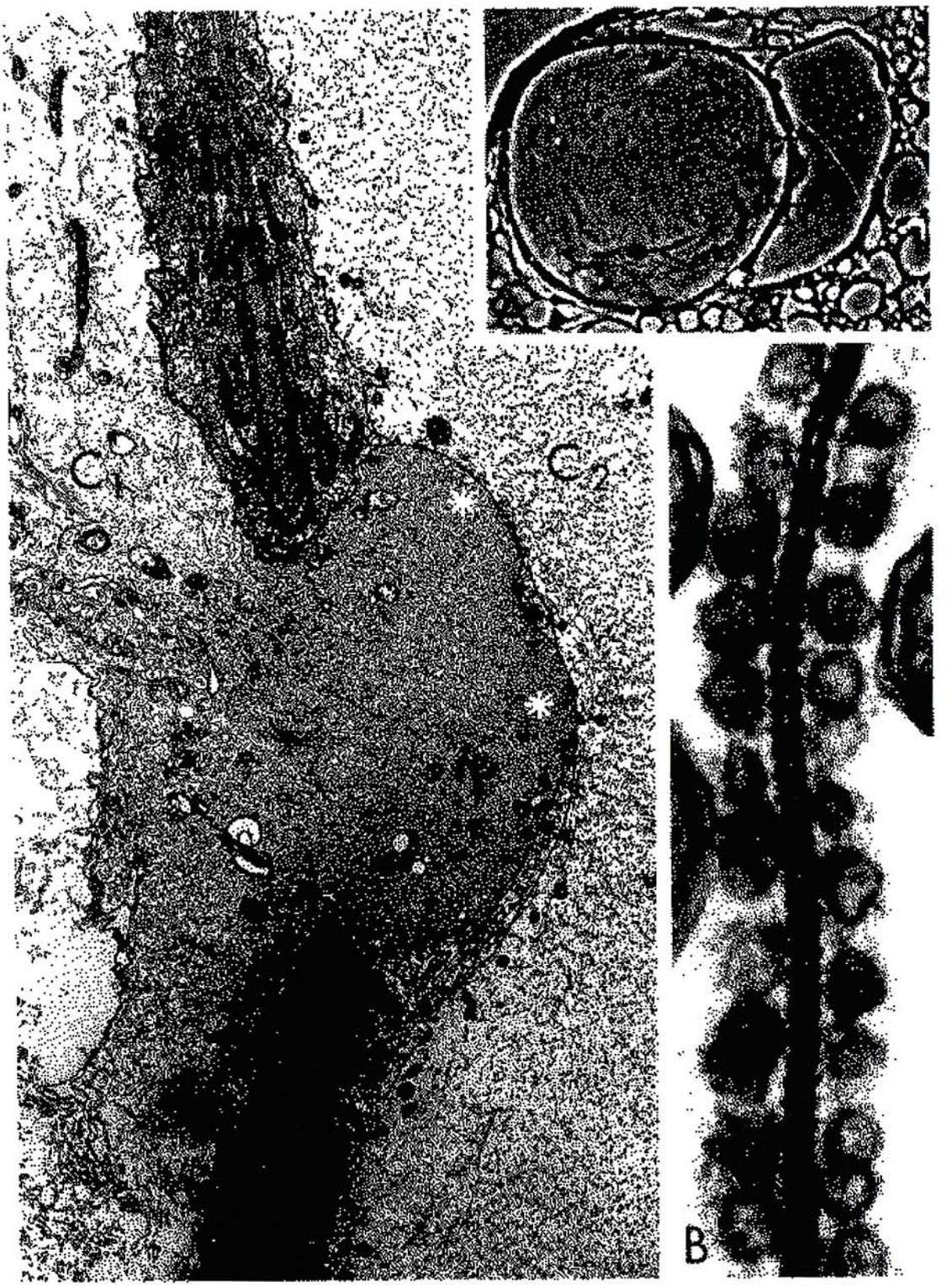

Figure 2.3: Ultrastructure of gap junctions at a septum between crayfish lateral giant axons[49].

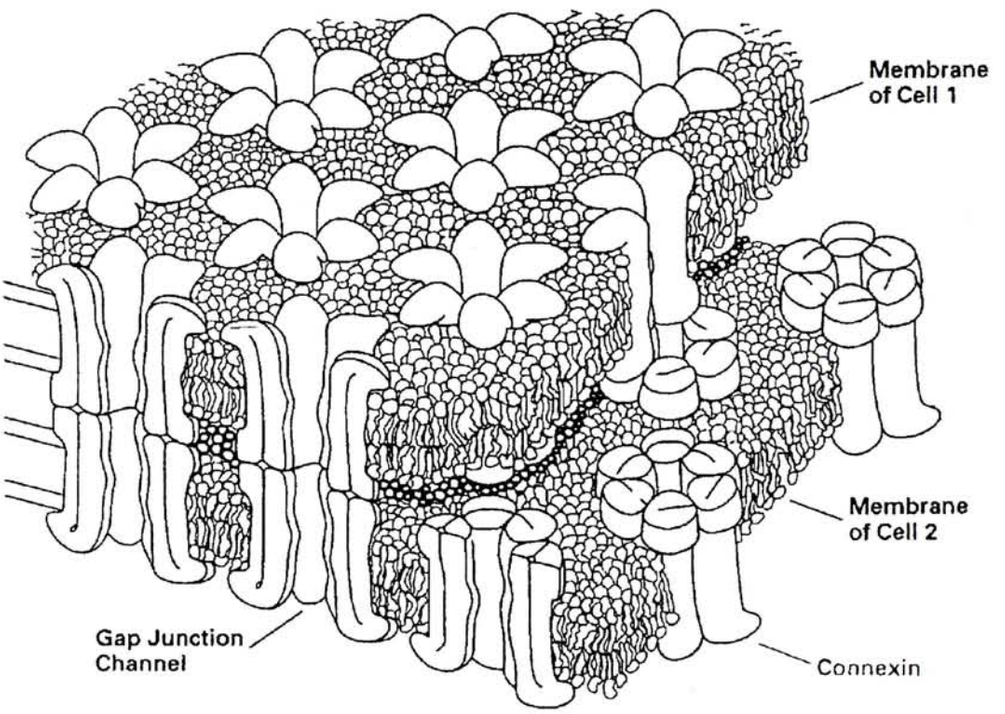

Figure 2.4: Gap junctions. Pores spanning two cell membranes are made of connexin proteins.

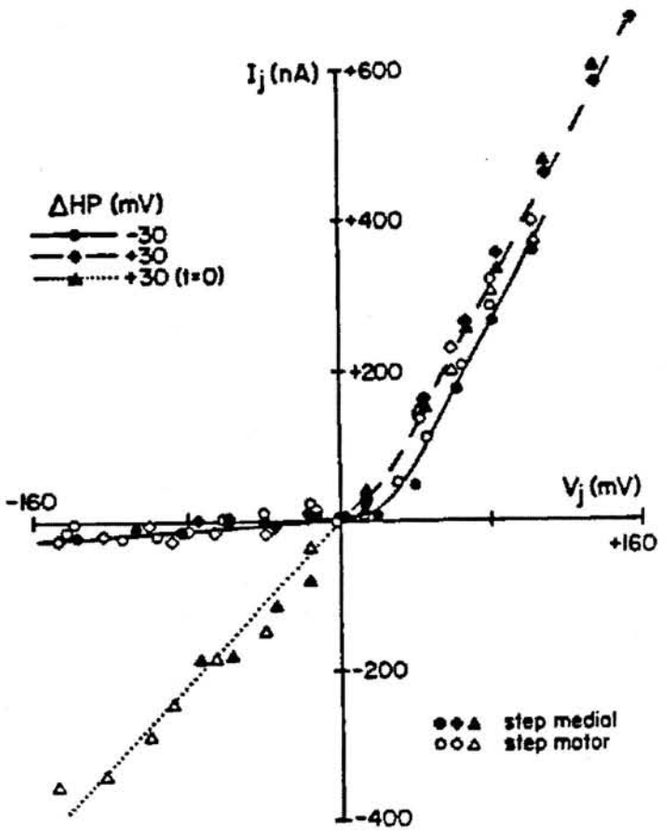

Figure 2.5: Double-voltage-clamp records and corresponding I-V curves demonstrating the peripherally directed current rectification of a perfused motor junction situated between a medial and a motor giant axon.

In our theory, the junctional capacitance, C_j, is mainly caused by the capacitance between the channels. If doing a cross-section over the 3-d gap junction patch in Fig. 2.4, we may obtain the digram shown in Fig. 2.6.

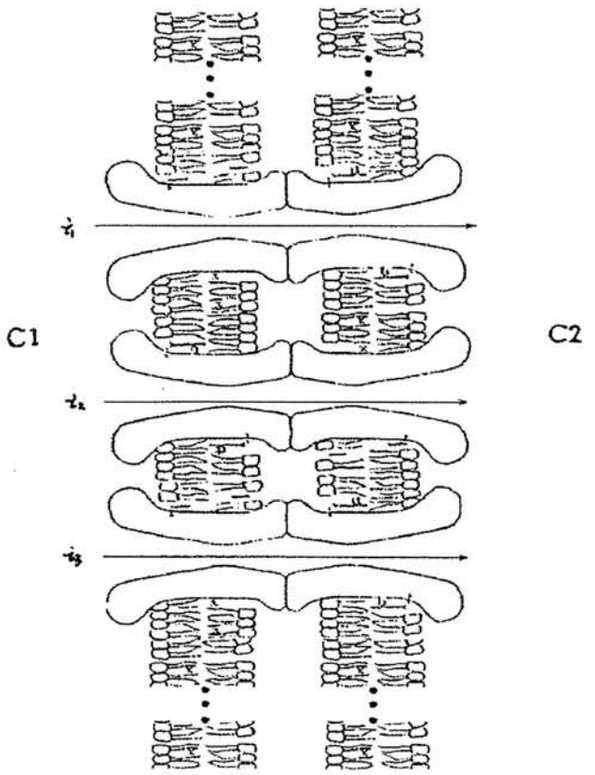

Figure 2.6: A schematic diagram of three neighbored channels of the gap junction.

When the signal, generally AC, transmitting through the gap junction, the current from the pre-synapse is branched into i_1, i_2 and i_3 which are insulated by the wall of the channels. Thus the intermedia between the channels, such as the wall of channel, the membrane where the channels embedded and the extracellular fluid in the cleft between the pre- and post- synaptic membrane, will act as the intermedium of a capacitor. Since the channels at the gap junction are parallel to each other, they are electrically connected in parallel with the same transjunctional voltage also. The discrepancy between the channels, mainly in the diameter and in the individual channel resistance, is the reason for the

current difference in each channel. Thus at the same axial position between the channels the voltage difference exists there. Therefore during the ionic current transmission across the gap junction, there must be some current "leaks" away into the extracellular fluid. For convenience, the capacitance between the channels is modeled by an assembled capacitor as the macroscopic reaction at the gap junction, which is in consistent with the assembled resistance here. The density of the channels distributed at the junctional area and the diameters of channels are the main factors that affect the transmitting properties at the gap junction, like resistivity and capacitivity. Once the value of this parameters changed, the different extent of peak delay, peak attenuation and duration change at the post-membrane will be caused.

2.3 Numerical Calculation

1. Calculating the action potential of pre-synaptic membrane V(t) at point a.

The F-H equation is described as follows:

$$I = I_i + I_c; \tag{2.9}$$

where

$$I_i = I_{Na} + I_K + I_p + I_L, \tag{2.10}$$

$$I_{Na} = P_{Na}\frac{EF^2}{RT}\frac{[Na]_o - [Na]_i exp(EF/RT)}{1 - exp(EF/RT)}. \tag{2.11}$$

I_p and I_K are computed from similar equations with appropriate concentrations and permeabilities.

$$P_{Na} = \bar{P}_{Na} h m^2, \tag{2.12}$$

where

$$\frac{dm}{dt} = \alpha_m(1 - m) - \beta_m m, \tag{2.13}$$

and

$$\frac{dh}{dt} = \alpha_h(1 - h) - \beta_h h. \tag{2.14}$$

$$P_p = \bar{P}_p p^2, \tag{2.15}$$

where

$$\frac{dp}{dt} = \alpha_p(1 - p) - \beta_p p. \tag{2.16}$$

$$P_K = P'_K n^2, \tag{2.17}$$

where

$$\frac{dn}{dt} = \alpha_n(1 - n) - \beta_n n. \tag{2.18}$$

The parameters in the F-H model are illustrated in the Table.2.1.

Parameter	Description
$[Na]_o$; $[Na]_i$	outside and inside sodium concentration
G	membrane conductance
P_{Na}	sodium permeability
$[K]_o$;$[K]_i$	outside and inside potassium concentration
P_k	potassium permeability
P_p	non-specific permeability
I_{Na}	sodium current
$\bar{P}_{Na}$	sodium permeability constant
I_K	potassium current
P'_K	potassium permeability constant
I_L	leak current
$\bar{P}_p$	non-specific permeability constant
I_i	ionic current
g_L	leak conductance
m	variable for sodium permeability
C_m	membrane capacitance
E_{Na}	sodium equilibrium potential
h	variable for inactivation of sodium permeability
E_p	non-specific current equilibrium potential
n	variable for potassium permeability
p	variable for non-specific permeability

Parameter	Description
E_L	leak current equilibrium potential
$\alpha;\beta$	rate constants for m, h, n and p as indicated by suffix
R	gap constant
T	absolute temperature
$A; B; C$	empirical constants in equations for $\alpha's$ and $\beta's$
F	Faraday's constant

Table 2.1. The parameters used in F-H model

The values of α's and β's at a certain potential are given by the following equations, with the values for the A, B and C given in the data list:

$$\alpha_h = A(B-V)/\{1-exp((V-B)/C)\}, \tag{2.19}$$

$$\beta_h = A/\{1+exp((B-V)/C)\}, \tag{2.20}$$

$$\alpha_m = A(V-B)/\{1-exp((B-V)/C)\}, \tag{2.21}$$

$$\beta_m = A(B-V)/\{1-exp((V-B)/C)\}. \tag{2.22}$$

α_p and α_n are given by equations similar to Equ. 2.21 and β_p and β_n by equations similar to Equ. 2.22.

$$I_L = g_L(V-V_L) \tag{2.23}$$

$$I_c = I-(I_{Na}+I_K+I_p+I_L), \tag{2.24}$$

$$\frac{dV}{dt} = \frac{I_c}{C_m}. \tag{2.25}$$

	A	B	C
	$(msec^{-1})$	(mV)	(mV)
α_h	0.1	-10	6
β_h	4.5	+45	10
α_m	0.36	+22	3
β_m	0.4	+13	20
α_p	0.006	+40	10
β_p	0.09	-25	20
α_n	0.02	+35	10
β_n	0.05	+10	10

Table 2.2. Different values for A, B, C in F-H calculation

$[Na]_o = 114.5mM$	$E_r = -70mV$	$\bar{P}_{Na} = 8 \times 10^{-3} cm/sec$
$[K]_o = 2.5mM$	$g_L = 30.3mmho/cm^2$	$\bar{P}_p = 0.54 \times 10^{-3} cm/sec$
$[Na]_i = 13.74mM$	$V_L = 0.026mV$	$P'_K = 1.2 \times 10^{-3} cm/sec$
$[K]_i = 120mM$	$C_m = 2\mu F/cm^2$	

standard initial values: $V = 0mV$; $h_0 = 0.8249$; $m_0 = 0.0005$; $p_0 = 0.0049$; $n_0 = 0.0268$.

F-H model is a first order non-linear differential equation. In order to solve the equation, the Runge-Kutta forth order method is used and the numerical method is implemented by Matlab. The magnitude of the input current is set at 1000 $\mu A/cm^2$ with the duration of 0.1ms, the standard stimulation in this work, which is enough to bring out an excitation at the pre-membrane where the threshold current intensity is near 510-550$\mu A/cm^2$. Fig. 2.7 shows this threshold of the F-H membrane block as well as its "all-or-none" property. The amplitude of membrane potential varies with the increase of stimulating intensity like a step function. The step around 510-550$\mu A/cm^2$ may be considered as the threshold for

the membrane, When the the stimuli are less than this value the reaction of the membrane is subthreshold, while above this value the reaction will be an action potential. The computed value V(t) is then used as the input to the junction part of the model.

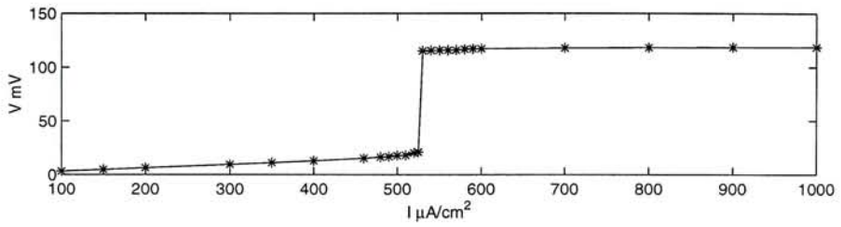

Figure 2.7: The "all-or-none" property of the F-H block given square current wave with magnitude $1000\mu A/cm^2$ and duration $0.1ms$ as its stimulation.

2. Calculating the current flowing into the post-membrane. The part of the current caused by the voltage difference between points a and c acts as the stimuli to the post-membrane F-H unit which is connected in parallel with the capacitor C_j. For the values of R_j given, the quantity of the total current flowing into the post-membrane unit and C_j is figured out by $\frac{V_c - V_d}{R_j}$.

3. Calculating the voltage change of the post-membrane unit. The change in the post-membrane potential is calculated for the given current in ac branch computed in step 2, and it is used as the stimuli to the post-membrane. Again upon using Runge-Kutta forth method, the voltage waveform is obtained by solving the F-H equation at the post-membrane in which the value of C_m is replaced by the combined value of C_j with the membrane capacitance, when the current flowing in ac branch orthordromicly.

2.4 Simulation Results

According to the calculation method stated in the previous section, Fig. 2.8 shows the calculated curve obtained at the pre-membrane when given the standard stimulation and those at the post-membrane with the fixed value of the R_j while varied capacitance of the C_j. Fig. 2.9 is computed with the same parameter setting as that of Fig. 2.8 except we fix the value of the C_j but change the resistance of the R_j[52]. Fig.2.11 is the experimental records at the GMS of crayfish[28]. It is clear that both R_j and C_j can achieve the peak delay and the peak attenuation at the post-membrane. However, it is suggested in Fig. 2.10 that only increasing the value of C_j will cause the increased duration at the post-potential. The increased duration at the post-potentials in Fig. 2.9 are caused by C_j induced in the model.

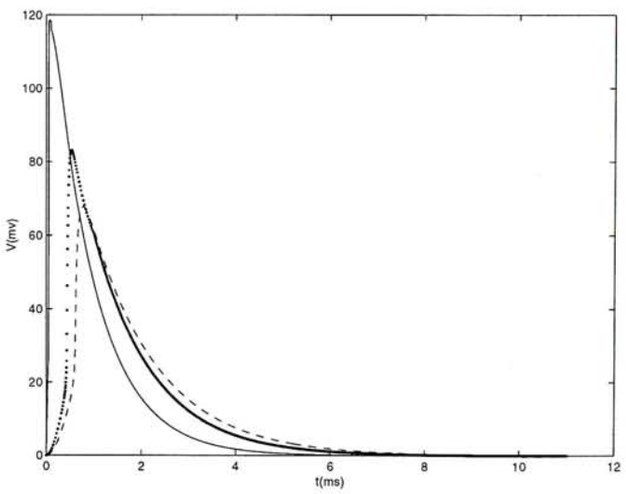

Figure 2.8: The calculated curves for pre- and post-membrane. The solid curve is for pre-membrane with the standard stimulation; the other two are obtained at the post-membrane with the fixed value of R_j=50$\Omega \cdot cm^2$ while varied capacitance of C_j, the dotted line with C_j=10μF/cm^2 and the dashed line with C_j=20muF/cm^2.

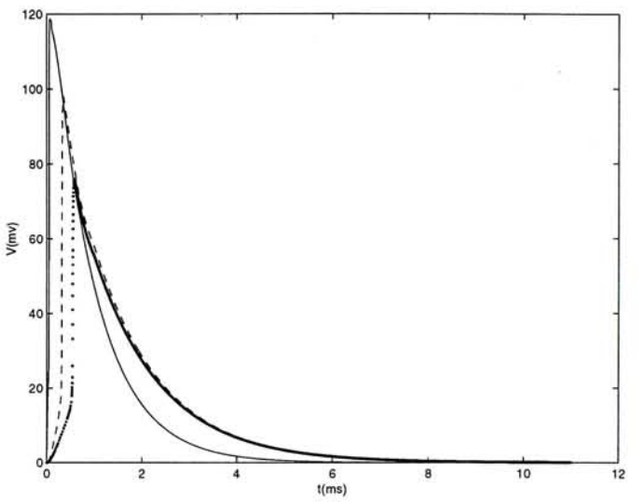

Figure 2.9: The calculated curves for pre- and post-membrane. The solid curve is for pre-membrane with the standard stimulation; the other two are obtained at the post-membrane with the fixed value of C_j=2μF/cm^2 while varied resistance of R_j, the dotted line with R_j=180$\Omega \cdot cm^2$ and the dashed line with R_j=200$\Omega \cdot cm^2$.

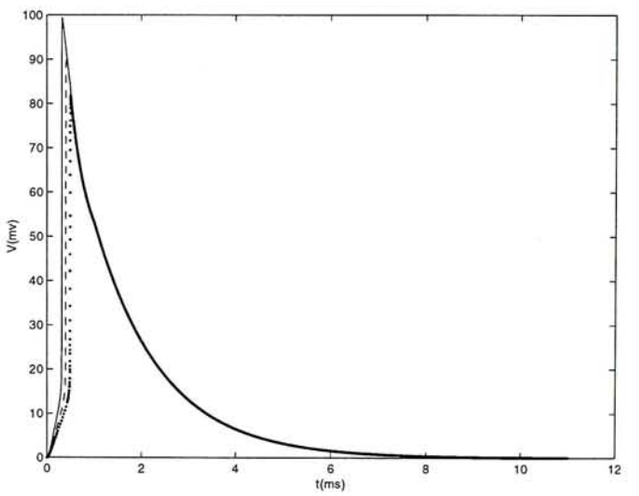

Figure 2.10: The calculated curves for pre- and post-membrane. The solid curve is for pre-membrane with the standard stimulation; the other two are obtained at the post-membrane without taking into account of the value of C_j, the dashed line with R_j=180$\Omega \cdot cm^2$ and the dotted line with R_j=200$\Omega \cdot cm^2$.

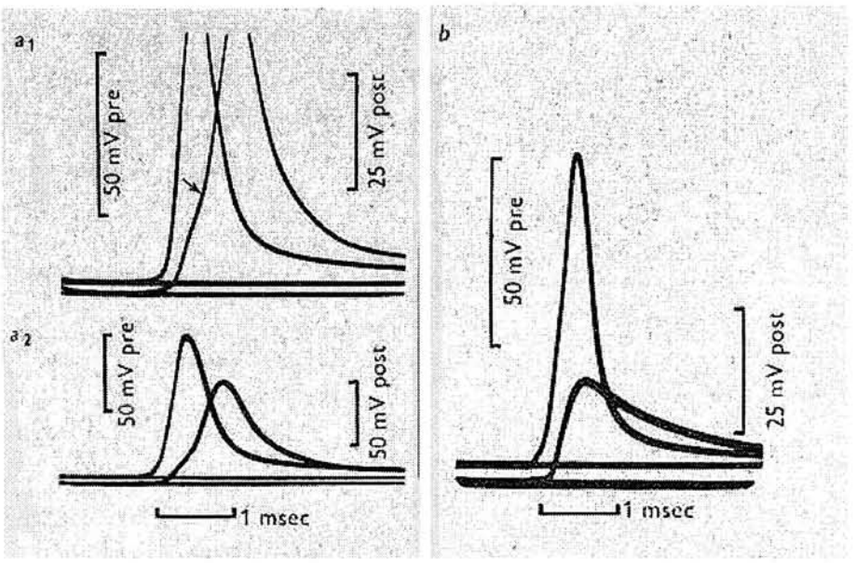

Figure 2.11: The experimental records at the GMS of crayfish[28].

We did a set of simulation with different values of C_j or R_j while fixed the other parameter in the model, in order to speculate the individual functions of C_j and R_j on the action potential transmission. Given a constant action potential generated at the pre-membrane, Table.2.3 describes the peak attenuation, V_{at}, and the peak delay, T_d, caused by C_j, which is obtained by fixing $R_j = 20\Omega.cm^2$ while varying C_j from $5\mu F/cm^2$-$30\mu F/cm^2$. The values for C_j are in the same order as C_m, the membrane capacitance, usually it is equal to $1\mu F/cm^2$. While Table.2.4 is the data for the peak attenuation and the peak delay caused by R_j, increasing gradually from $20\Omega/cm^2$ to $140\Omega.cm^2$, when given C_j is equal to $20\Omega.cm^2$. The variation range for R_j is consistent with the data reported in Furshpan's work[28]. Fig. 2.12 and Fig. 2.13 are the summary over the two tables. Comparing to the action potential generated at the pre-membrane, the dashed lines depict the change of the time delay and the solid lines reflect the peak attenuation of the post-potentials given different parameter setting.

$C_j, \mu F/cm^2$	V_{at}, mV	T_d,msec
5	0	0
7	6.99	0.08
8	10.87	0.125
9	14.75	0.17
10	18.5	0.21
11	22.25	0.25
12	25.7	0.3
15	35.25	0.42
17	39.83	0.51
20	45.75	0.64
22	48.85	0.74
25	52.8	0.89
27	55.1	1
30	58.09	1.17

Table 2.3. Data collection of peak attenuation and peak delay when fixing$R_j = 20\Omega.cm^2$

$R_j, \Omega.cm^2$	V_{at}, mV	T_d,msec
20	0	0
25	2.05	0.035
30	4.41	0.06
35	6.63	0.08
40	8.76	0.1
45	10.82	0.12
50	12.84	0.13
55	14.8	0.15
65	18.66	0.19
75	22.44	0.23
85	26.1	0.27
95	29.74	0.31
105	33.27	0.36
140	45.4	0.56

Table 2.4. Data collection of peak attenuation and peak delay when fixing$C_j = 5\mu F/cm^2$

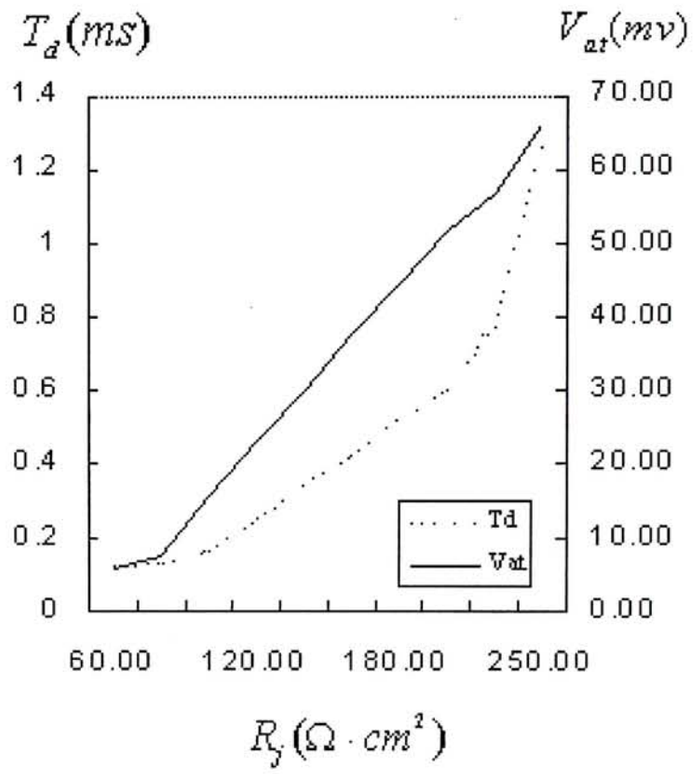

Figure 2.12: The attenuation and the peak delay with the change of R_j. The dashed lines are the curves of the peak time delay T_d between the post-potential and the pre-potential; and the solid lines are the curves of peak attenuation V_{at} of the post-potential with respect to the pre-potential.

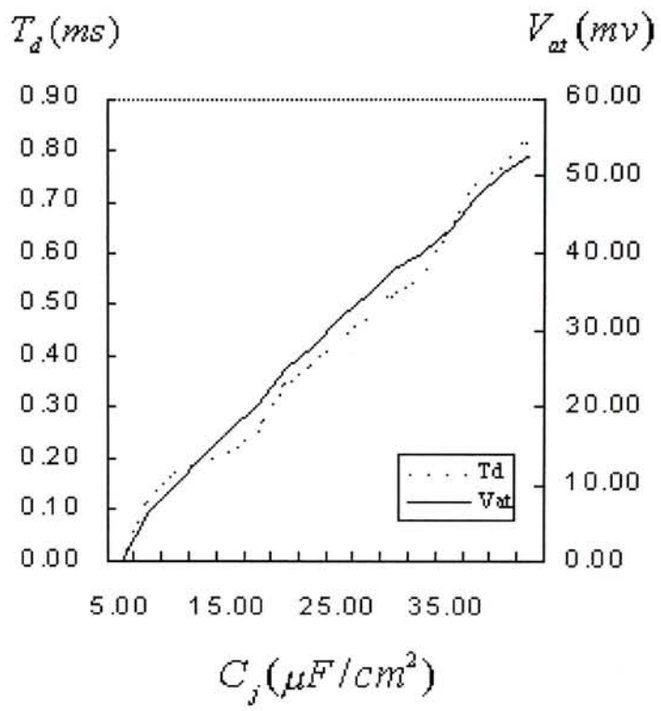

Figure 2.13: The attenuation and the peak delay with the change of C_j. The dashed lines are the curves of the peak time delay T_d between the post-potential and the pre-potential; and the solid lines are the curves of peak attenuation V_{at} of the post-potential with respect to the pre-potential.

2.5 Discussion

Fig. 2.11 is the simultaneous intracellular recordings from pre- and post-fibers in the experiment[28]. In each case pre-fiber potential was recorded on the upper trace. Comparing the action potential observed at the pre- and the post-membrane, there is an obvious delay of the peak time and the increased duration of the post-potential. Fig. 2.11.a_1 and a_2 were the same data but recorded with different amplification. In Fig. 2.11.a_2, the peak attenuation at the post-potential is clear to see.

Comparing the experimental records with the simulation action potentials produced by the model, the similar peak delays and the peak attenuations are achieved by the model as the post-potentials given in both Fig. 2.8 and Fig. 2.9. The peak delay at the post-potential observed in the experiment is around $1ms$, and the peak delay acheived by our model is also within the same range when the values of parameters are in the reasonable physiological scope as illustrated previously. From the statistical results in Fig. 2.12 and Fig. 2.13, it is suggested that the increases of the value of either C_j or R_j will reduce the amplitude of the action potential obtained at the post-membrane and the peak delay as well. While from the simulated post-potentials shown in Fig. 2.8 and Fig. 2.9, the post-potentials obtained by increasing R_j only are slightly different in shapes from those calculated corresponding to larger C_js. With larger values of C_j, the post-potentials not only display the peak attenuation and the peak delay but also the in creased duration as observed in the experimental records. From the simulation results, however, it seems that the additional resistance at the gap junction only reduces the peak amplitude and the time to peak of the post-potential.

In other gap junction models, like the one-dimensional cardiac model developed by Cartee and Plonsey in 1992, the gap junction which connected two cardiac

cells together is modeled only by a pure linear resistor. While as introduced in the section of introduction and in the chapter 1, the duration dispersion recorded at the post-membrane in the tissues where arrhythmia occurs is the most intriguing symptom in the cardiovascular diagnosis. Although in the very beginning the model in our work is not developed for cardiac tissue especially, the mechanism of the information transmission at the gap junction of GMS and that of heart are the same. Since both of them conduct the nerve impulses by direct electrical transmission through the gap junctional channels. From the simulation results in our work, it indicates that junctional resistance is a necessary component for the gap junction model, however, it is not the only one to tell the whole story of the gap junction, at least it can not achieve the increased duration of the post-potential.

The simulation results and the statistical data only give the primary information about the functions of C_j and R_j that in the synaptic model. To theoretically study how C_j and R_j affect the behavior at the gap junction is the next step we did in our work. The theoretical analysis on the model will be introduced in the chapter that follows.

Chapter 3

Analysis of the Synaptic Model

This chapter details an analysis of the rectifying electrical synapse model. An introduction is given below, followed by the time constant analysis, a comparison between the model developed in our work and the model of Giaume's, and finally there is a discussion.

3.1 Introduction

The wide distribution and conservation of connexins in different cells and organisms, as well as their modulation at both transcriptional and protein levels, indicate their fundamental importance for cell function.

Aberrations in connexon expression have been implicated in cancer, cardiac ischemia, and cardiac hypertrophy. Recently, exciting new insights into the structure and function of gap junction channels have emerged from human genetics. These studies have implicated gap junctions in two inherited human diseases; Charcot-Marie-Tooth(CMT) which is a disease of peripheral nerves that affects both motor and sensory nerve functions and visceroatrial heterotaxia syndrome (VAH)[53]. The gap junction channel defects in these diseases provide models for

gap junctions channel dysfunction, and they provide important new perspectives about the role of connexins in development and physiology. It is also proposed in the growth control hypothesis by Loewenstein emphasizes the possibility that growth regulatory signals are transmitted through gap junctions[54]. Implicit in this hypothesis was that a decreased communication capacity would lead to uncontrolled growth in the extreme cases, such as occurs in cancer. In most cases the dispersion in the duration of the post-potentials will be detected in the defect of cell communication.

As it has been mentioned in Chapter 1 that the goal of the modeling is trying to relate the structure to the function. Different models for gap junctions provide us the understanding of the mechanism from different angles. However, until now, the study on the gap junction models are still stopped at the level of the measurements of the junctional resistance, even for the analysis on the pathological cases that mentioned above. It is believed that the histological changes in the failed tissues may only lead to the change of the junctional resistance. Correspondingly, a lot of statistical data on the detected junctional resistance have been reported in many research works over the last several years[55][56]. The decoupling of the cells communicating via gap junctions dose increase the junctional resistance. It is indicated in last chapter that the change of the values of C_j and R_j will both cause the peak delay and the peak attenuation at the post-membrane, however, the duration of the post-potential is only affected by the value of C_j. The section that follows is the analysis of the morphology of the post-potential from the view-point of the time constant.

3.2 Time Constant Analysis

3.2.1 Junctional Time Constant in Bennette's Model

In Bennett' study on the physiology of electrotonic junctions including the GMS of the crayfish, the model developed for the coupling cells is given in Fig. 3.1[32]. In this model, the two coupling cells have a portion of their surface membranes in contact where gap junction is formed. The resistivity of the cytoplasm and external medium are ignored. The two cells and the junction are each represented by a lumped resistance and capacity. V_1 will be considered as the pre-membrane potential which is clamped at both C_1 and r_1[32] and V_2 as the post-membrane potential. C_c is the so-called junctional capacity in his model and it is negligible as stated in his report.

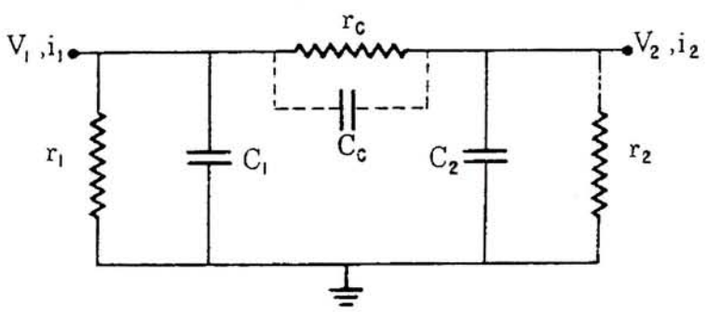

Figure 3.1: The model for an electrotonic junction in Bennett' work. The pre-membrane and the post-membrane are only assumed inactive and represented by the passive membrane model.

In the circuit C_2 and r_2 are the capacitance and the resistance of the post-membrane respectively. When calculating the output cross-membrane voltage, V_2, it was assumed for simplicity that V_1 could be clamped to an arbitrary $V_1(t)$ and effectively $r_1 = 0$. The differential equation for the equivalent circuit becomes:

$$\frac{V_2}{r_2} + C_2\dot{V}_2 = \frac{1}{r_c}(V_2 - V_1) + C_c(\dot{V}_1 - \dot{V}_2), \tag{3.1}$$

where $\dot{V}_i$ is the first differentiation of the voltage with respect to time. The time

constant of the junctional coupling is

$$\tau = \frac{r_c r_2}{r_c + r_2}(C_c + C_2), \tag{3.2}$$

Since in Bennette's work, C_c can be ignored, there came out the conclusion that the time constant of junctional membranes was usually short compared to the post-junctional time constant. Then according to Bennette's model comparing to an action potential that occurs at the non-synaptic membrane or the action potential that occurs at the pre-membrane, it will not be the peak delay and the increased duration observed at the post-membrane, but the shortened duration and the peak advance will appear at the post-potential given a constant action potential at the pre-membrane. Furthermore in that study, the peak time of the post-potential is only depended on the peak time of the input action potential from the pre-membrane. A coefficient, α, appeared in the input action potential and was defined as the ratio of the coupling time constant to the rise time or time to peak of the impulse function. Fig. 3.2 shows the post-potential changes with different values of α.

In Bennette's model the peak delay of the post-potential is not a characteristic of the gap junction but a changeable parameter set by modeler. Moreover, as indicated by Bennette himself, when C_c was considered into the model, the diphasic post-potential would be obtained as given in Fig. 3.3, and the peak time of the post-potential therefore would be more advanced than the pre-potential due to the high-pass effect induced by C_c. However, it was reported in Peter Getting's work that what they detected in the experiment was that the gap junction had the low-pass characteristic[40]. The misleading results in Bennette's work partly is due to the limitation of the misunderstanding at the gap junction histologically and physiologically in 1960's. The freeze fracture technique, which reveals the structure of gap junctions, was invented in 1970's, and the study of the connexin

expression prospers only in the recent years.

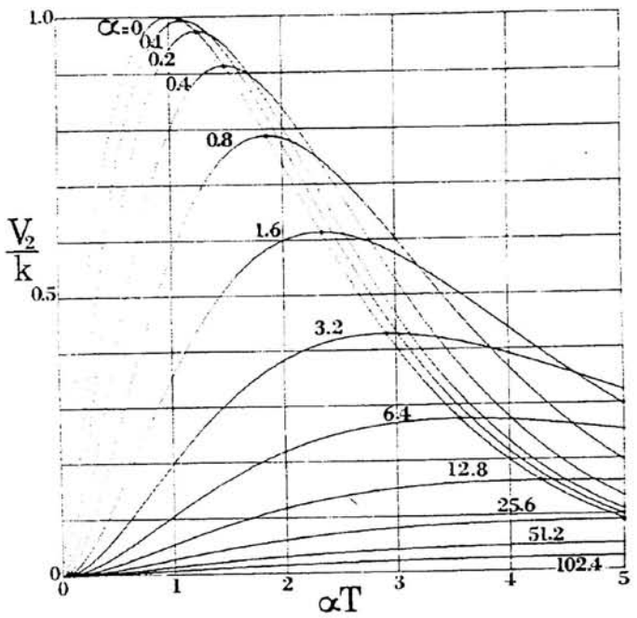

Figure 3.2: Postjunctional potential, V_2, obtained by Bennette's model without considering C_c.

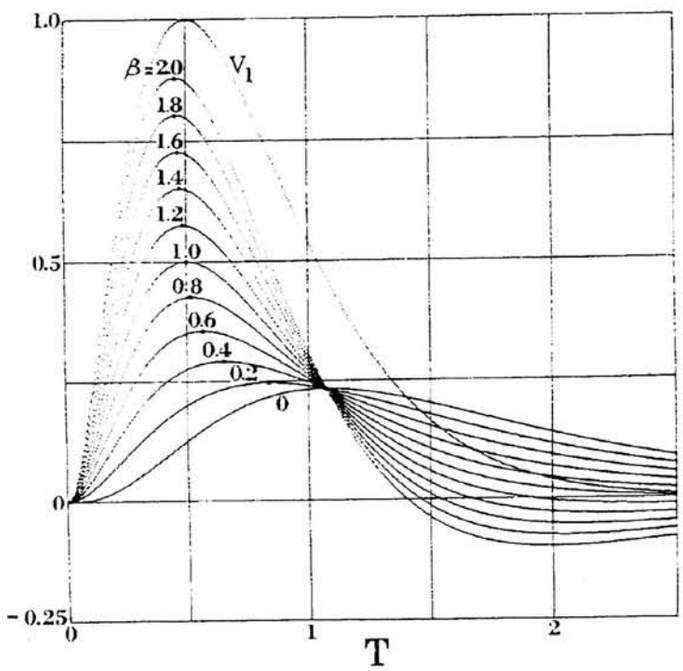

Figure 3.3: The diphasic postjunctional potential, V_2, obtained by Bennette's model when the junctional capacity, C_c, is not negligible.

3.2.2 The Junctional Time Constant in Our Model

Although the results given in Bennette's model somehow deviate from the experimental data, the time constant analysis is a quite useful measure to qualify the action potential transmission at the gap junction especially in the study of post-potential duration changes. Intuitively, the duration increase in the post-membrane potential and the rounder peak appears in the post-potential are considered as the increased time constant during the action potential transmission through the gap junction. In order to verify this idea, we simplify the original circuitry model into the circuit given in Fig. 3.4[57].

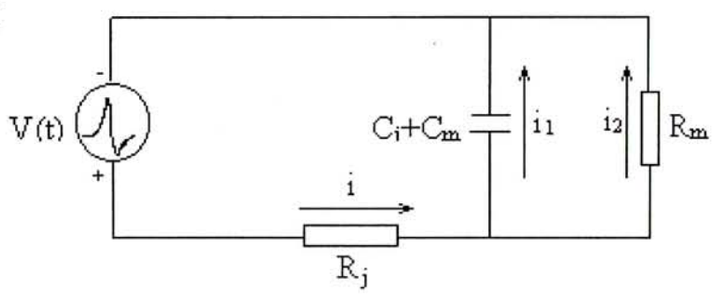

Figure 3.4: The simplified circuit with post-membrane only having passive characteristics.

In the theoretical analysis on the time constant at the gap junction, the post-membrane in the model may be simplified that only has passive property and is modeled by the parallel connection of C_m, membrane capacitance, and R_m, membrane resistor, as shown in Fig. 3.4. Since time constant is a concept for the passive transmission. If the action potential coming from the pre-membrane is V(t), the current and voltage relationship in the circuit may be described by a series of equations as in Equ. 4.5,

$$\begin{aligned} \frac{1}{C}\int i_1(t)dt + i(t)R_j &= V(t) \\ \frac{1}{C}\int i_1(t)dt &= i_2(t)R_m \end{aligned}$$

$$i_1(t) + i_2(t) = i(t). \tag{3.3}$$

After doing the simplification over Equ. 3.3, Equ. 3.4 is obtained to explain the relationship between the current flowing along the R_m branch and the voltage across the post-membrane.

$$CR\frac{di_2(t)}{dt} + i_2(t) = \frac{1}{R_j + R_m}V(t), \tag{3.4}$$

where $C = C_m + C_j$ and $R = \frac{R_m R_j}{R_j + R_m}$ which is the equivalent resistance for parallel connected R_m and R_j. The production of CR may be considered as the time constant τ at the gap junction, which is determined not only by the parameters of the gap channels but also those of membrane where the channels embedded. The equivalent resistance of R should be less than either R_j or R_m, which will lead to the smaller time constant, compared with the general membrane time constant of neurons, if C_j is negligible or even dose not exist. However, such smaller time constant will cause peak advance but not peak delay as it has been discussed in analysis of Bennette's model. Therefore the time constant at the gap junction must be larger than that of general membrane's. It is needed to have a compensation from the other component, C, in the time constant to increase the value. Since C_m is a constant for the membrane, the only flexible factor is C_j which may contribute to the larger junctional time constant.

There is another factor should be taken into account when doing the analysis on the action potential transmission at the gap junction. It is the value for the resistivity of the post-membrane, which will not be as large as that when membrane is inactivated during an action potential occurs. The consequence of this is the equivalent resistance composed by R_j and R_m in parallel will be much smaller.

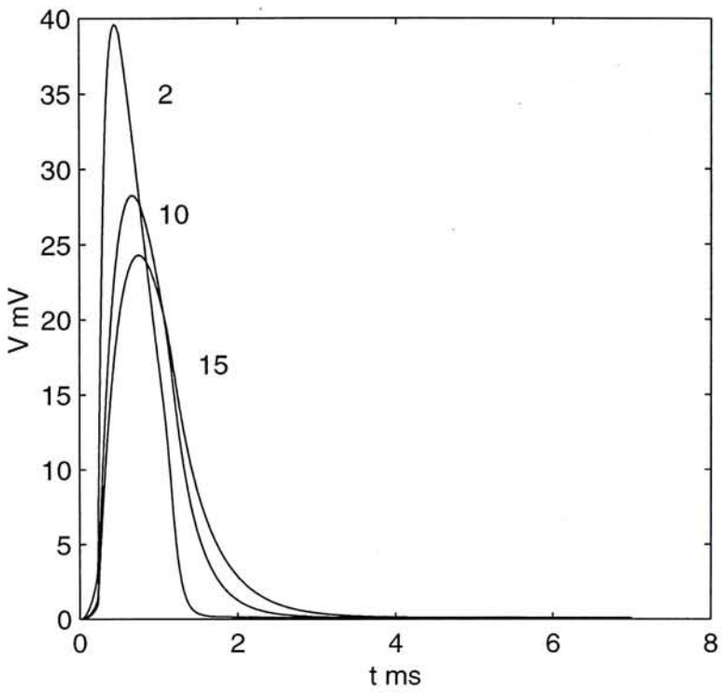

Figure 3.5: The variation of the post-potential duration with different values of C_j. The three curves in the figure are calculated with $C_j = 2, 10, 15\mu F/cm^2$ given $R_j = 60\Omega.cm^2$

Since when the membrane is depolarized, which is the case in the signal transmission at the gap junction, the membrane resistance R_m will decrease, and the extreme value $23\Omega.cm^2$ was recorded in 1947[58]. In this work R_m is assumed to be $50\Omega.cm^2$ as the value selected for R_j ranging from $60\Omega.cm^2$ to $200\Omega.cm^2$. Therefore the value of the junctional resistance R_j actually has less contribution to the control of the time constant at the junctional part than we used to consider it did. Fig. 3.5 shows the effect of C_j on the post-potential duration, and Fig. 3.6 displays the variation in the shape of post-potentials when R_j changes. It is obvious that R_j can not control the larger duration in the normal post-potential that recorded in the experiment, and increasing R_j only reduces the amplitude of the post-potentials.

The early stage of fibrosis and calcification of the cardiac cells may be considered as the major cause of the time constant increasing at the cardiac gap

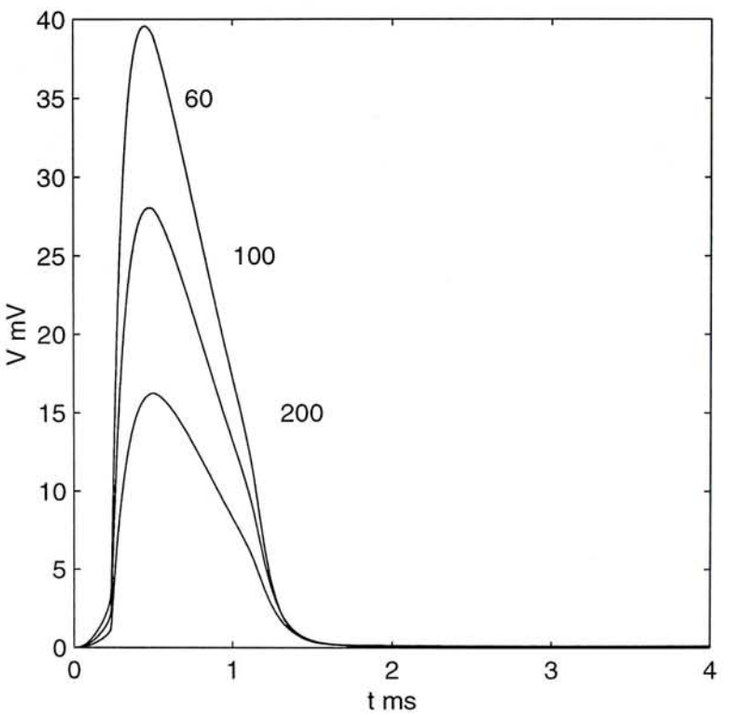

Figure 3.6: The variation of the post-potential duration with different values of R_j. The three curves in the figure are calculated with $R_j = 60, 100, 200\Omega.cm^2$ given $C_j = 2\mu F/cm^2$.

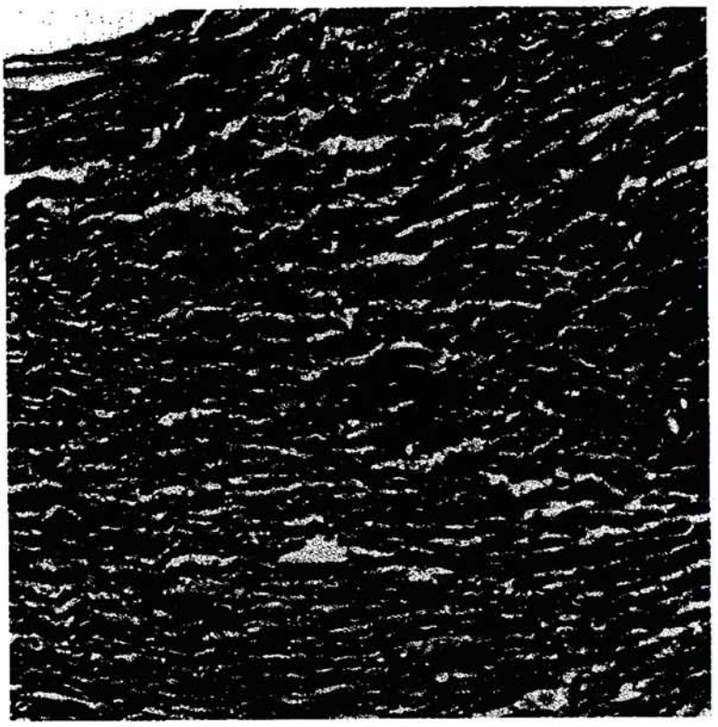

Figure 3.7: Normal histological findings of the right ventricle of control hamster(11 months old) Haematoxylon-eosin; magnification 50x[59].

junctions. Histological studies performed in normal and CM hamsters indicated extensive areas of interstitial fibrosis and calcification in the myopathic ventricle but not in the normal animal, as given in Fig. 3.7 and Fig. 3.8[59], and severe destruction of intercellular contacts can be seen in the right and left ventricle of cardiomyopathic hamsters using confocal microscopy. In these fibrosis tissues, the dispersion of the post-potential durations was observed. The failed tissues will not only increase the resistance of the gap junction but also will increase the medium that between the gap junction channels, which will cause the increase of the capacitance there.

3.3 Model Reconstruction

Giaume's model

In Giaume's work, the same rectifying crayfish giant motor synapse was studied, using the double-voltage-clamp technique which allowed direct measurements of junctional current at various fixed transjunctional potentials[34].The objective of that work is to obtain more detailed information about this particular synapse, GMS, and also to determine if the 'synaptic-rectifier' hypothesis postulated by Furshpan and Potter is supported by the properties of the over-all population of junctional channels. In addition, the use of the double-voltage-clamp technique allowed both the pre- and the post- membrane potentials to be fixed at constant level, thereby excluding non-specific changes in electrotonic coupling induced by non-junctional membrane currents[60]. The simultaneous and independent control of both membrane potentials allowed a quantitative assessment of the respective effects of the transjunctional and the transmembrane voltages, on the junctional conductance.

However, due to the limitation of the double-voltage-clamp itself, the results of Giaume's only reveal the steady-state of the transjunctional chord conductance as indicated in that report. Yet the data provided in that report support the notion that the synapse consists of channel-like elements whose opening and closing with the transjunctional voltage give the junction its 'diode'-like behavior.The transjunctional potential, V_j, was calculated by subtracting the membrane potential of the motor fiber, V_2, from that recorded in the lateral axon, V_1, so that $V_j = V_1 - V_2$. Under voltage clamp, when one side of the junction was held at its resting potential, any changes in the clamping current monitored on that side was due solely to current originating from the junction. For example, if V_1 was maintained at the resting potential of the lateral giant axon while V_2 was

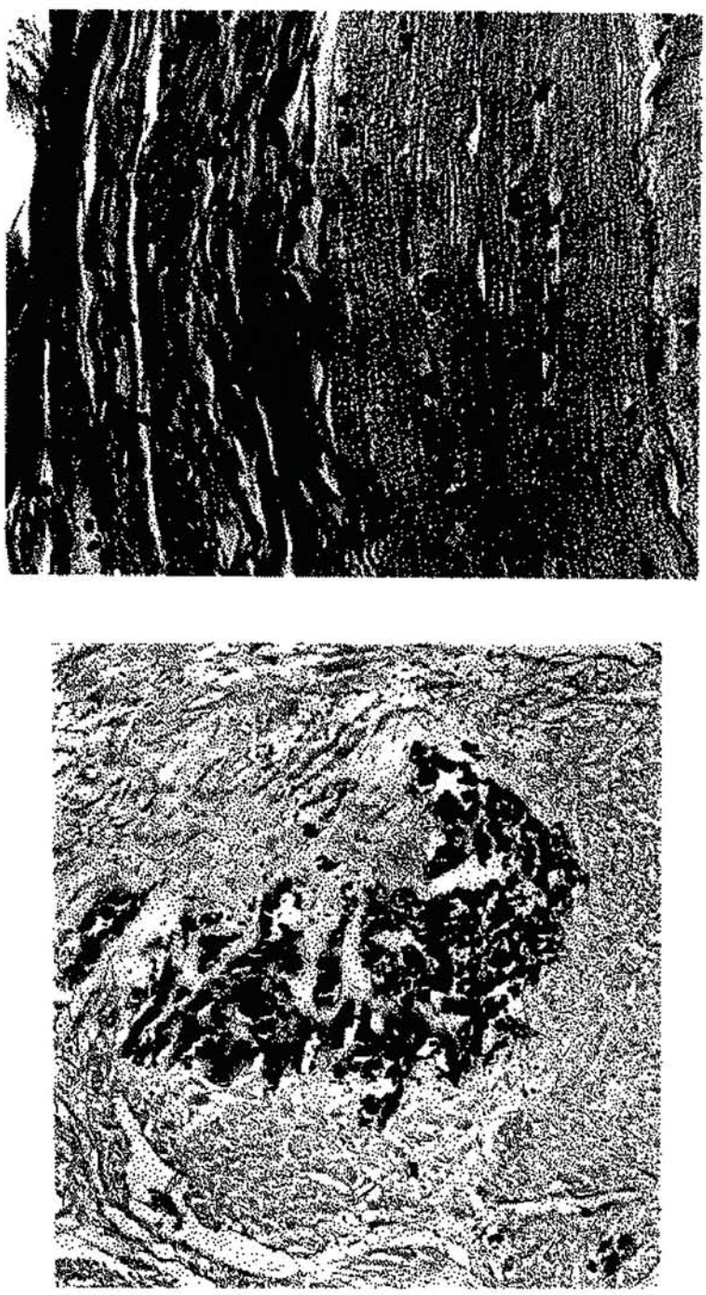

Figure 3.8: Top-Histopathology or the right ventricle of cardiomyopathic hamster(11 months old) showing extensive interstitial fibrosis with Masson trichrome. Magnification 50x. Bottom-Von Kossa's stain of the left ventricle of cardiomyopathic hamster (11 months old) showing central lesion with Ca depots[59].

stepped to various levels, I_1 recorded was equal and opposite in sign to the total junctional current, I_j, for the resulting V_j.

The experimental chord conductances, g_j, were calculated for each measured value of the steady-state junctional current I_j, according to the relation $g_j = I_j/V_j$. Their values were then fitted to the Boltzmann relation, using the following modified version:

$$g'_j = (\frac{g_{max} - gmin}{1 + exp[-A(V_j - V_0)]}) + g_{min}, \tag{3.5}$$

in which g_{min} and g_{max} are the minimum and maximum conductances, respectively. The parameters A and V_0 are constants expressing the voltage sensitivity, and the transjunctional potential at which $g_j = 1/2g_{max}$, respectively.

The voltage-sensitivity constant A was calculated from

$$A = -ln(\frac{g_j - g_{min}}{g_{max} - g_j})/(V_j - V_0), \tag{3.6}$$

for each V_j and its corresponding G_j. Since both V_0 and A were unknown, they were estimated reiteratively by adjusting V_0 to obtain the least standard deviation for A over the positive range of V_j values. The constant in that work are: $A = 0.15 \pm 0.03mV^{-1}$ and $V_0 = 28 \pm 4mV$.

The transjunctional conductance calculated by the Boltzmann equation is given in Fig. 3.9

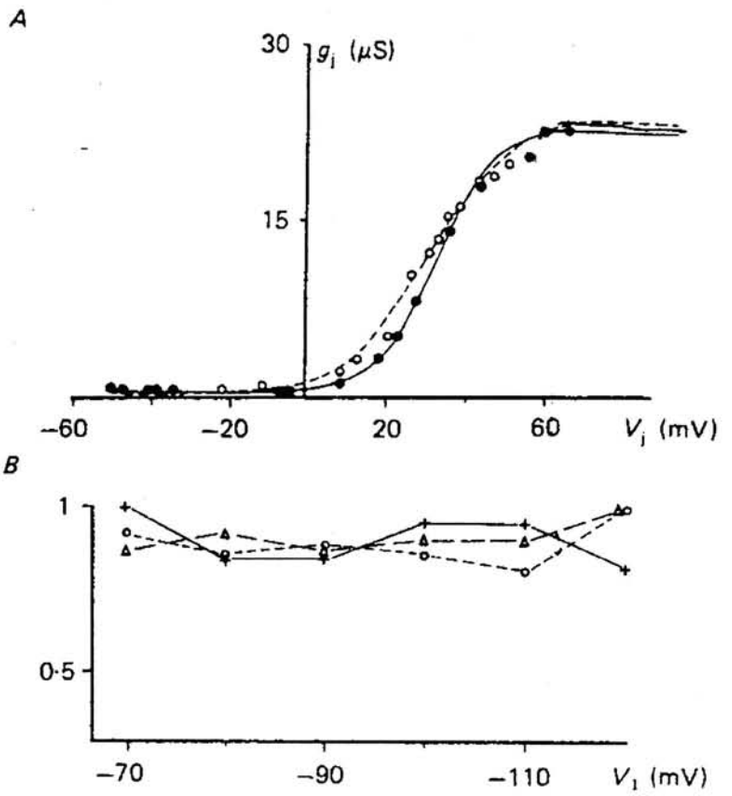

Figure 3.9: Junctional conductances calculated with different parameter setting reported in Giaume's work in 1987[34].

The Circuitry Model

In Giaume's work the existence of C_m can not be detected. It is because when the pre- and the post- membrane are clamped at fixed values and in their steady states, the currents in the channels are DC. Thus there will be no leaky current flowing away from the C_m. The characteristics illustrated by Giaume's model can be reconstructed by the combination of R_j and D_j, if D_j is not ideal.

The I-V characteristic of the diode can be given by

$$I = I_s(e^{(V-V_0)/V_T} - 1). \tag{3.7}$$

In the Equ. 3.7, V_0 and V_T bear the same meaning as V_0 and A that in Giaume's model do. The nonlinear conductance of the diode may be obtained by

differentiating I with respect to V,

$$g_d = \frac{dI}{dV}. \tag{3.8}$$

Therefore the total conductance of the gap junction will be

$$g_j' = \frac{g_j g_d}{g_j + g_d}, \tag{3.9}$$

where g_j is the reciprocal of R_j. Fig. 3.10 compares the result calculated by Boltzmann function and that calculated by the circuit model. It should be noted that in our circuitry model the resistors, both R_j and R_m, represent the resistivities and have the dimension, $\Omega.cm^2$. The area of the gap junction of GMS has the order $10^{-4}cm^2$[28]. Therefore, when we do the comparison between Giaume's model and ours, the conversion of the conductance from the density to the lumped value is necessary. The value selected for the area of gap junction in our work is from $1 \times 10^{-4}cm^2$ to $9 \times 10^{-4}cm^2$ in order to obtain a better results. There is a little shift between the two voltage dependent curves. It is because that the conductance calculated by Boltzmann function is lifted up by the constant value of g_{min} in the function. While in our model g_{min} is treated as zero. Fig. 3.11[34] and Fig. 3.12 are the I-V relationship detected in the experiment and the result reconstructed by our model.

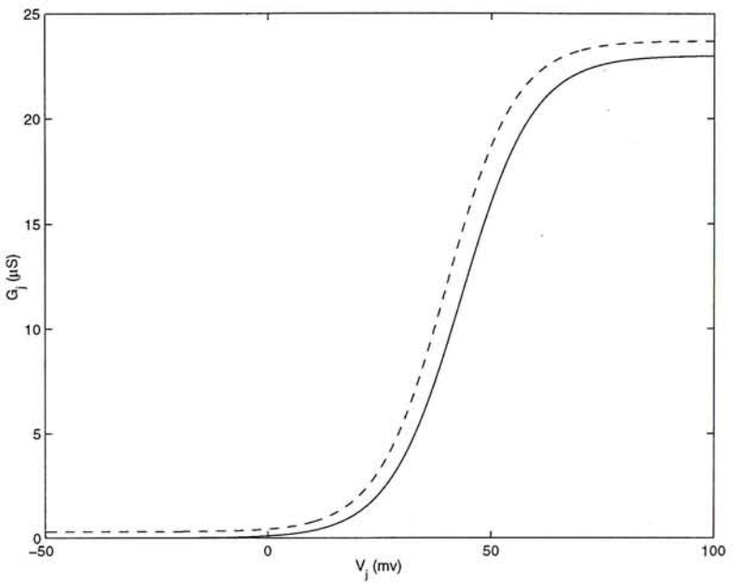

Figure 3.10: The comparison between the voltage-dependent conductance calculated using the Boltzmann function and the new circuit model. The dashed line is the result by the Boltzmann function with $V_0 = 40mV$ and $A = 0.13mV^{-1}$; and the solid line is the result by the circuit model with $V_0 = 20mV$ and $V_T = 8mV$, the area of gap junction is $10^{-4}cm^2$ in the calculation.

3.4 Discussion

It is also mentioned in Giaume's work that the spike at the post-membrane is evoked more likely by the peak of the pre-potential but not its rising phase.[34] If this phenomenon is explained by the existence of the C_j then it is easy to understand. Under the detecting condition of the double-cell voltage clamp used in that experiment, the cross junctional voltage V_j has the synchronized rising phase and the peak with those of the pre-potential. When V_j is in its rising phase, most of the junctional current will be shunted away by the C_j into the extracellular because of the considerable value of the first order differentiation. However, when the cross junctional voltage reaching to its peak, its first order differentiation is equal to zero. It also means that the current flowing in the C_j branch is zero at this instant when the current generated by the cross junctional voltage will totally flowing into the post-synapse and be strong enough to evoke

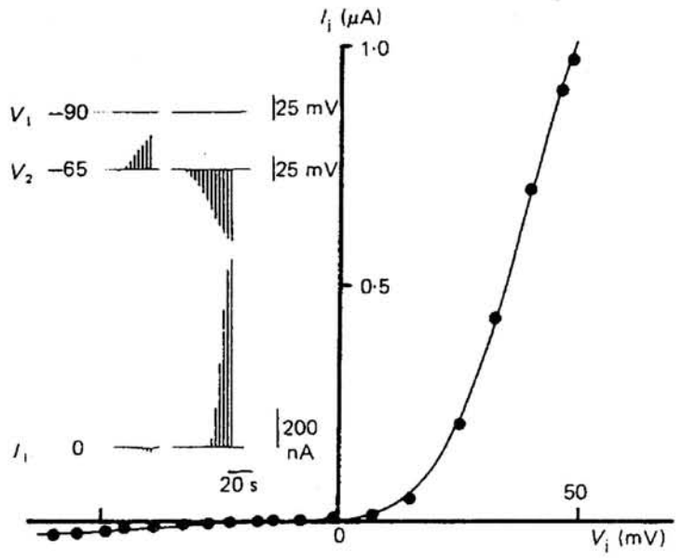

Figure 3.11: Junctional rectification demonstrated with voltage steps from resting potential. Inset, V_1 and V_2 were held at the indicated potentials and I_1 was recorded for voltage pulses of about $750ms$ long applied in V_2. The junctional current I_j was measured at the end of each step. Graph, plot of I_j versus the transjunctional voltage $V_j = V_1 - V_2$.

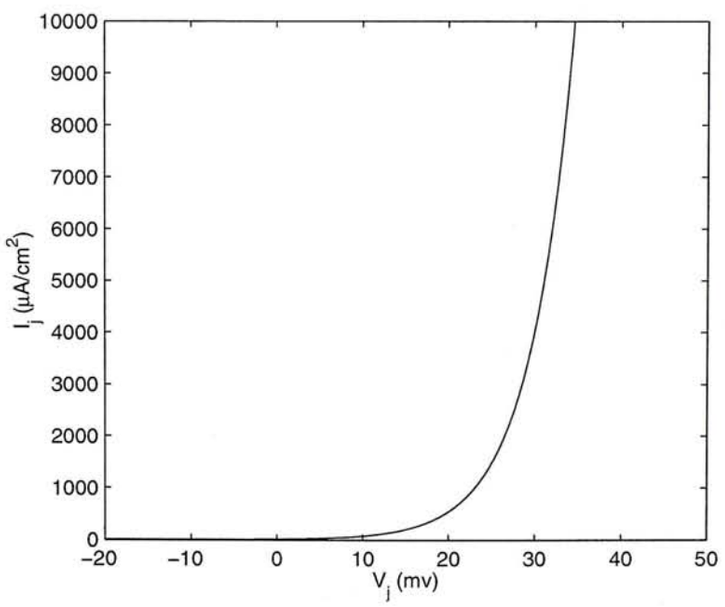

Figure 3.12: The I-V relationship reconstructed by our circuitry model, when selecting $V_0 = 10mV$, $V_T = 5mV$ and the area of gap junction is $10^{-4}cm^2$.

an action potential there. This is the observed delay of the post-potential.

If the increasing of the time constant at the post-membrane is not due to the extra capacitance but the resistance then such delayed post-potential is hard to explain. Since no matter in which phase during an action potential the current flowing through the shunting resistor, if existing, will always be proportional to the voltage. That implies, even in the rising phase, an action potential is most likely to be evoked. It is no need to wait until the peak arrives, because the threshold is easy to exceed if comparing to the amplitude of the action potential. An other evidence for the existence of C_j is the low pass characteristic detected by Getting[40]. Nevertheless, in that paper the low pass characteristic is explained by capacitance of the post-membrane and the junctional resistance. While if it was the case, the increased time constant at the gap junction could not be achieved. Since the parallel connected junctional resistance and post-membrane resistance has the value which is less than the post-membrane resistance only. The time constant at the gap junction is comparatively smaller than that of the membrane. Therefore, by Getting's theory, it is the shorter duration, sharper peak and no peak delay that would be obtained at the post-membrane.

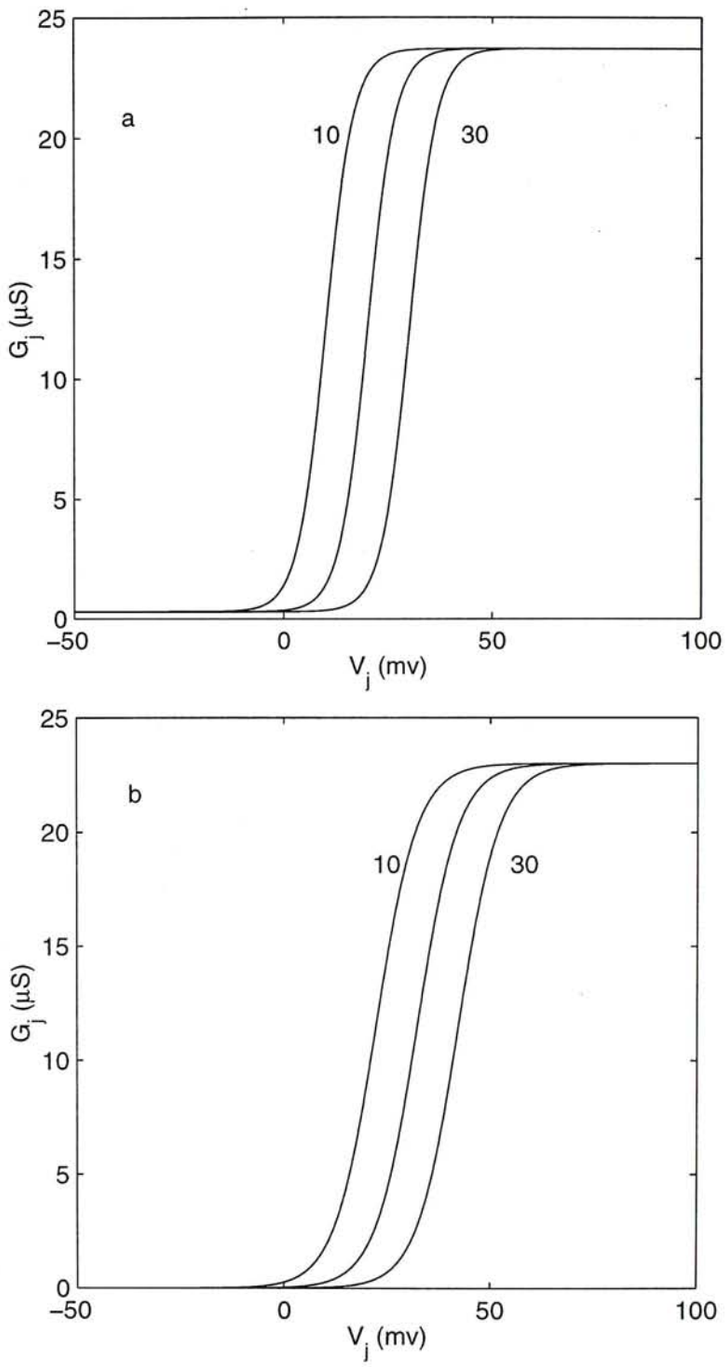

Figure 3.13: a. The threshold shifting in Giaume's model, when $V_0 = 10, 20, 30mV$ given $A = 0.5mV^{-1}$. b. The threshold shifting reconstructed by out model, when $V_0 = 10, 20, 30mV$ given $V_T = 5mV$.

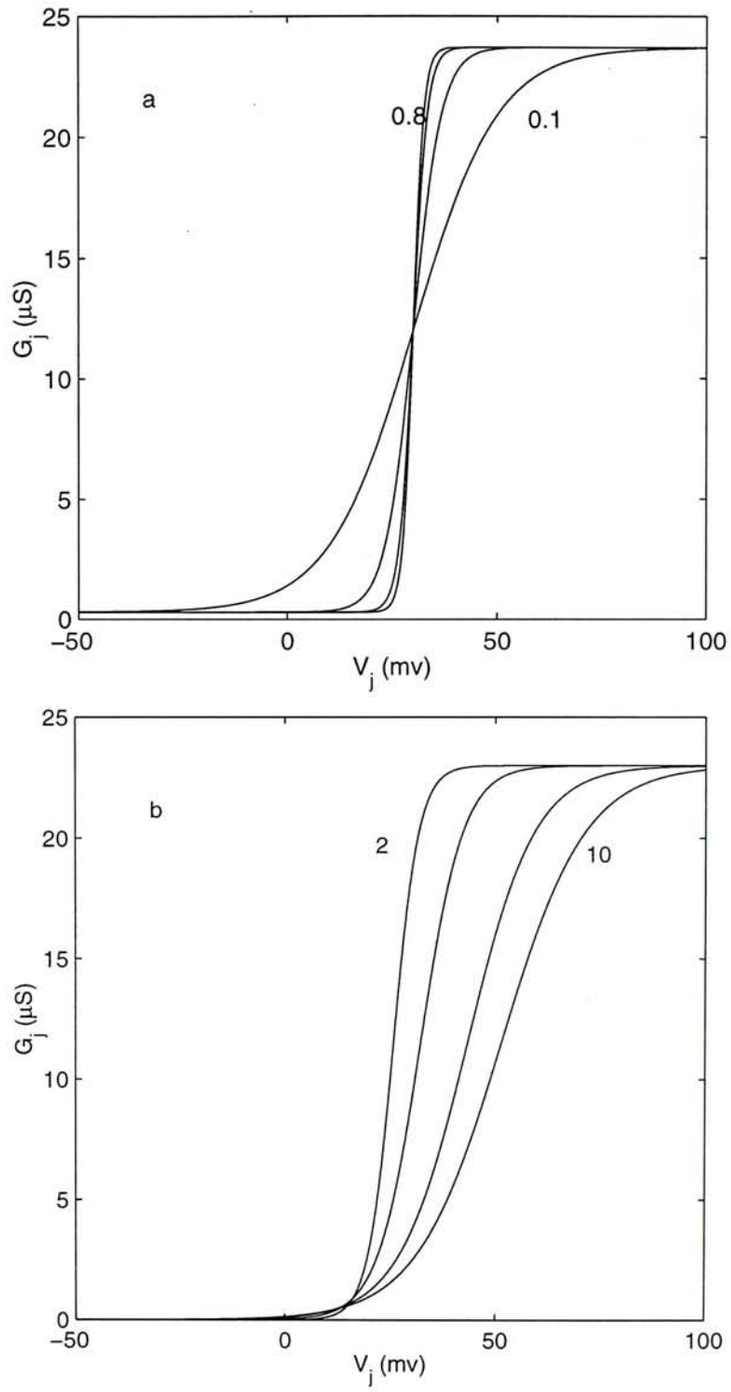

Figure 3.14: a. The adjustment of the sensitivity by Giaume's model, when $A = 0.1, 0.3, 0.6, 0.8mV^{-1}$ given $V_0 = 30mv$. b. The adjustment of the sensitivity reconstructed by our model, when $V_T = 2, 4, 6, 10mV$ given $V_0 = 20mV$.

Model reconstruction wise, it is found that the threshold V_0 and the sensitivity parameter A are two important parameters. While V_0 controls the voltage at which the junctional conductance will reach to the half of the maximum, and A determines the steepness of the conductance with respect to the cross-junctional voltage. As shown in Fig. 3.13, the threshold V_0 determines the position of the "gate" of the gap junctional conductance. While in Fig. 3.14, it show how the sensitivity A in the two models control how fast the gap junctional gate reaches to its maximum. The variation ranges for A and $\frac{1}{V_T}$ are the same for achieving the similar voltage dependent junctional conductance. The difference between Giaume's and ours is the definition for the position of the threshold. in Giaume's model the threshold is at the voltage where $g_j = 1/2 g_{max}$ while in our model the threshold is equal to the transjunctional voltage when $g'_j = \frac{g_j I_s/V_T}{I_S/V_T + g_j}$.

There is an interesting result observed from Giaume's model is if let $V_0 = 0mV$ and the sensitivity is set to a large very, say $1mV^{-1}$, the Giaume's model will behave like an ideal diode connected in series with a resistor, as shown in Fig. 3.15. This discovery suggests that on description of the steady state behavior of the electrical synapse, GMS, our model is consistent with the model developed by Giaume's.

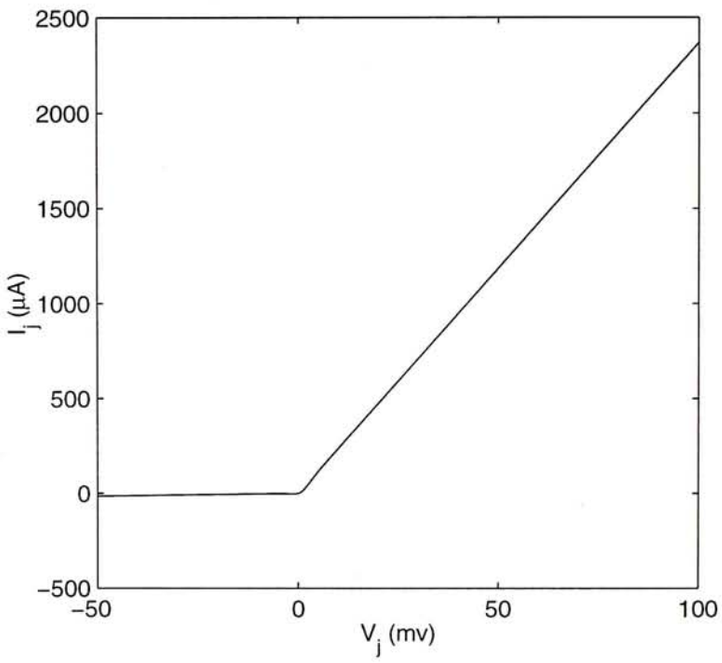

Figure 3.15: The I-V relationship at the transjunctional conductance in Giaume's model give $A = 1mV^{-1}$ and $V_0 = 0mV$.

Chapter 4

Action Potential Train Transmission Analysis

As cells go, neurons are not loners. Every function of the nervous system, from regulation of autonomic activities to the control of complex animal behaviors, reflects the coordinated action of a network of interacting neurons. In studies of the neural network, although many of the interactions among neurons occur through chemical synapses or local hormonal actions, an important category that must not be overlooked is networks in which the cells interact via electrical synapsed, mediated by gap junctions. In such networks, neurons are coupled electrically such that an action potential may propagate from one cell to the next with no chemical intermediary. In fact some of the cells like cells AB and PD in the stomatogastric ganglion, are electrically coupled and therefore tend to fire together during bursts[61]. As the basic connection structure of the neural network or cell-network, the gap junction is modeled and analyzed functionally when given an action potential as the input at the pre-membrane in the previous chapters.

However, in the real physiological cases, it is action potential trains but not individual action potentials like modeled in the previously act as the information

carrier in the nervous system. The firing pattern of the neurons usually are beating, bursting or firing with irregular IPIs as introduced in the first chapter. The study of signal transmission characteristics in this neural network with various firing patterns is the main focus in this chapter and it marks the beginning of the second part of our work: the analysis of action potential train transmission through the gap junction. This Chapter presents a probabilistic approach to relating input and output firing levels in the nervous system when the input action potential train is temporally irregular. In this chapter, we first analyze how the absolute refractory period affects the probability density function of the output action potential train when considering the input action potential train is homogeneous Poisson. Then the effects of the gap junctional elements of the model on the action potential train transmission are studied by computer simulation.

4.1 Theoretical Analysis on the Refractory Period at the Post-membrane

Refractoriness is a property associated with the excitable membrane. Its function is not very obvious when studying the single action potential transmission through the gap junction. However, refractory period, especially the absolute refractory period, will affect the IPIs of action potential trains generated on the membrane and also the action potential train transmission through synapses once the refractoriness between the two coupling cells are not consistent. In this section we use the methods in point process to analyze the effect of the absolute refractory period of the post-membrane on the action potential train transmission.

4.1.1 Introduction of Membrane Threshold and Refractory Period

As introduced in the first chapter, the all-or-none is an important feature for the excitable membrane. Although the amplitude of the action potential is generally independent of stimulus intensity, the latency, the time delay from the onset of the stimulus to the peak of the action potential, is a function of stimulus strength. As shown in Fig. 4.1[1], the stronger the stimulus the shorter the delay between stimulus and action potential. The peak delay at the post-potential cause by junctional resistance also maybe explained by this reason. We shall see that this strength-latency relationship, together with another phenomenon known as the refractory period, allows the encoding of stimulus strength in terms of the frequency of action potentials in the axon.

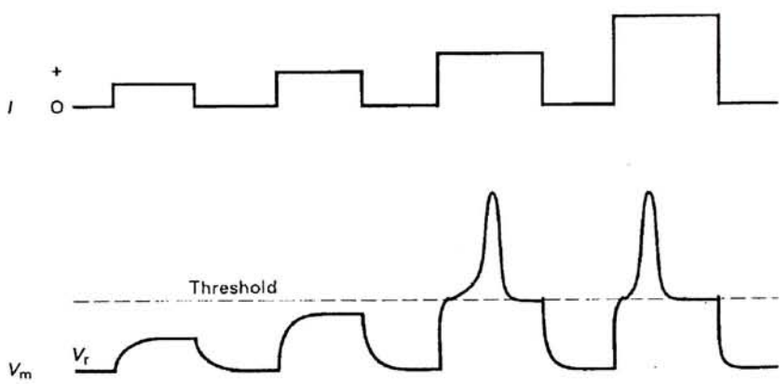

Figure 4.1: Active responses to small and large depolarizing stimuli. Although the above-threshold stimuli will cause action potentials, the latency will change according to the strength of the stimulus that applied.

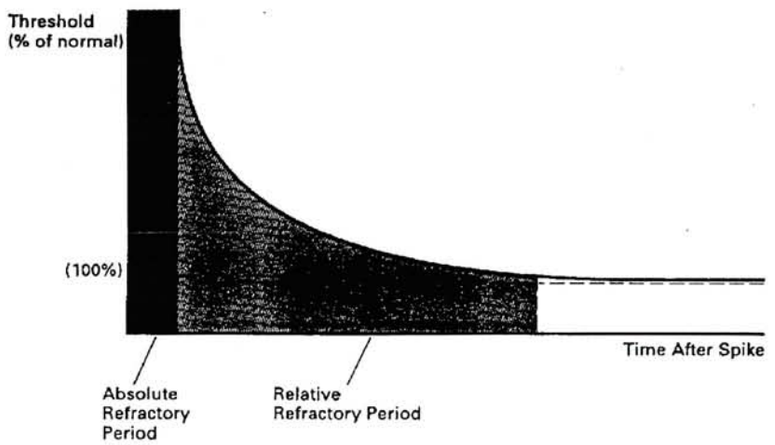

Figure 4.2: The threshold is not fixed. For a short period of time after the firing of an action potential, the threshold is much greater than normal.

For several milliseconds after the firing of an action potential, it is impossible to evoke another action potential no matter how large the depolarizing stimulus; in other words, the axon is refractory to stimuli during this time. This absolute refractory period is followed by a relative refractory period, during which the stimulus must be larger than normal to evoke and action potential. One useful way of thinking about the refractory period is in terms of the threshold. During the absolute refractory period the threshold is essentially infinite, and no stimulus, no matter how large, can exceed it. During the relative refractory period the threshold is larger than normal, that is it requires a larger than normal stimulus to exceed it. The threshold returns to the normal level with a time course shown in Fig. 4.2[62]; because only an above-threshold stimulus will evoke an action potential, this curve describes the stimulus strength required to generate a second action potential, especially the absolute refractory period, as a function of time after the first action potential. The refractory period is an important mechanism for the regulation of cell signaling that prevent the spreading of the misfiring which maybe caused by the noise from the pre-synapse. In many action potential trains are modeled as noisy pacemaker whose IPIs are normally distributed.

In such cases, the refractory period has special importance in regulation of the neuron firing. Therefore the refractory period is a necessary part which has to be considered in the study of action potential train transmission in the neural network.

4.1.2 Stochastic Models of Neuron Firing

Several mathematically oriented modelers have tried to use simple stochastic models to represent spontaneous firing in neurons[63]. These modelers have typically tried to predict the relative occurrence of time intervals of various durations between the adjacent action potentials in an action output potential train which is produced by applying the threshold rule to some assumed random distribution of input events[64].

In order to mimic the output action potential train conduction, certain concepts from the information sciences have been particularly useful in helping describe nervous activity. One can picture the dynamical activity of a nervous network as consisting of a large number of ongoing simultaneous time series of events (action potential trains) emerging from all the constituent cells. The output action potential train of any particular cell reflects the ongoing input trains at each of some several hundred of even thousands of synapses. Various synapses are weighted in significance according to the strength of the synaptic coupling between the pre- and the post-membrane. Consider first spontaneous firing activity in a single unit. One can characterize such activity by the rate of firing, the number of action potentials occurring perunit time. A somewhat more penetrating measure considers the set of interpulse intervals, i.e., the set of time intervals in, say, milliseconds, between adjacent action potentials in the train. This measure includes rate as a special case and also specifies the degree of regularity in the

firing pattern. A convenient way to display this information is the first-order interpulse-interval histogram. Suppose τ_i is the set of numbers which correspond to the time intervals between adjacent spikes in the train. The number of τ_i which fall in various size ranges are plotted against the size ranges themselves. This histogram approaches the probability density for interpulse intervals as the bin size for the time ranges approaches zero and can be considered as an approximation to it; i.e., the histogram measures the actual distribution of intervals in the train as they occurred, whereas the density function is an abstraction corresponding to the mathematical model one might adopt to describe the underlying process. Point process is one of the most efficient method for study the stochastic characteristics of the action potential trains

Point Process

Point processes are random processes which produce random collections of point occurrences, or series of events, usually (but not necessarily) along the time axis. In univariate point process analysis, the exact shape of the event is of no interest. The "time" of occurrence (or the intervals between occurrences) is the only information required. A more general case is the multivariate point process in which several classes of points are distinguished. In the multivariate case, the shape of the event serves only to classify it. The statistics of the process, however, are given in terms of the intervals only. Point processes can be viewed as a special case of general random processes and can be dealt with as a type of time series. Point processes analysis has been applied to a variety of applications ranging from the analysis of radioactive emission to road traffic studies and to queuing and inventory control problems. Point processes theory has been applied to the analysis of various biomedical signals[65][66]citeWatanabe. The main application, however, has been in the field of neurophysiology[68][69][70].

A neural action potential train is the sequence of action potentials picked up by an electrode from several neighboring neurons. The neurophysiologist is interested in the underlying cellular mechanisms producing the spikes. he may investigate, for example, the effects of environmental conditions such as temperature, pressure, or various ion concentrations or the effects of pharmacological agents. The analysis of the spike train may be used for the description, comparison, and classification of neural cells. Different interval patterns may result from the same cell under deferent conditions. Interneural connections may be investigated by analyzing the corresponding spike trains. Multivariate point processes analysis is sometimes required when the spike train contains action potentials from more than one neuron. Classification of each spike into one of the classes to be considered in the analysis is needed.

Once the events of the process have been defined, data is fitted into a point process model. The most often used models are renewal process, Poisson distribution, Gamma distribution, Weiball distribution.

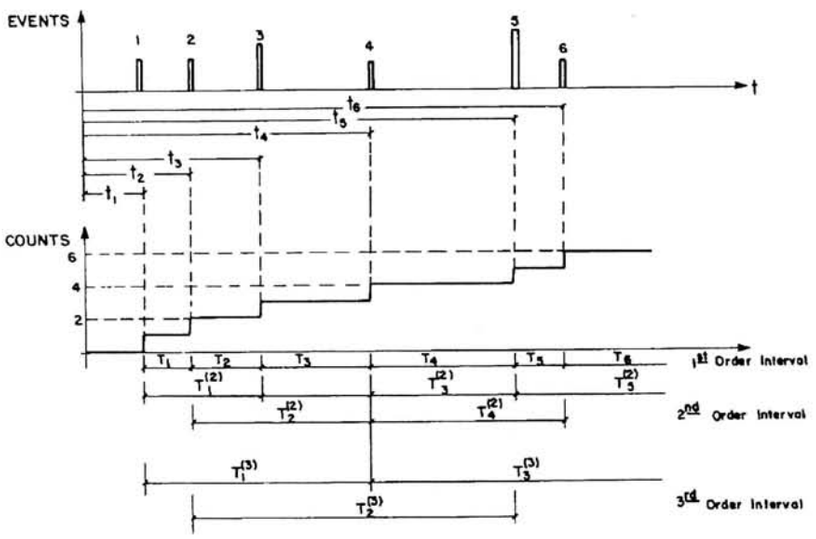

Figure 4.3: Events train

The point process is completely characterized by one or two of the canonical

forms: the interval process and the counting process. These are schematically described in Fig. 4.3. The interval process describes the time behavior of the events. The random times, t_i, $i = 1, 2, ...$ at which the ith event occurs is a way to describe the process. Here an arbitrary point in time is chosen as a reference. At this origin point, an event may or may not have occurred. The time intervals between two adjacent events, τ_i, $i = 1, 2, ...$, can also describe the process.

The event generating process is usually to be estimated, or modeled, with the aid of the finite time observed data. The various models are given in terms of the probability distribution functions. The motivation for modeling the point process is mainly to represent the event generation process in a concise parametric form. This allows the detection of changes in the process (due to pathology, for example) and comparison of samples from various processes.

Poisson Processes

An important class of point processes often used in modeling biological signals is the class of renewal processes. Renewal processes are processes in which the intervals between events are independently distributed with identical probability distribution function. In neural modeling it is commonly assumed that the action potential trains are renewal processes. Poisson processes are a special case of renewal processes, in which the identical interval distribution is a Poisson distribution. In the theory of point processes, the Poisson process, due to its simplicity, plays a somewhat analogous role to that of normal distribution in the study of random variables.

The Poisson process, with rate λ_0, is defined by the requirement that for all t, the following exists as $\Delta t \to 0$:

$$Prob\{N(t, t + \Delta t) = 1\} = \lambda_0 \Delta t + 0(\Delta t) \tag{4.1}$$

The constant rate, λ_0, denotes the average events per unit time or the meanfiring

rate. An important aspect of the definition in Equ. 4.1 is that the probability does not depend on time. The probability of having an event in $(t, t + \Delta t)$ does not depend on the past at all.

It is well known that for a random variable for which Equ. 4.1 holds, the probability of r events occurring in t (starting from some arbitrary time origin) is

$$Prob(N(t) = r) = \frac{(\lambda_0 t)^r}{r!} exp(-\lambda_0 t) \tag{4.2}$$

which is the Poisson probability. The probability of having zero events in time τ, followed by one event in the interval $\tau + dt$, is given by the joint probability of the two. However, the two probabilities are independent, due to the nature of the Poisson process. Also the probability of having one event in the interval $\tau + dt$ is by Equ. 4.1 $\lambda_0 dt$, hence,

$$p(\tau)dt = \frac{(\lambda_0 \tau)^0 exp(-\lambda_0 \tau)}{0!} \cdot \lambda_0 dt, \tag{4.3}$$

or

$$p(\tau) = \lambda_0 exp(-\lambda_0 \tau). \tag{4.4}$$

Equ. 4.4 gives the p.d.f. of the Poisson distribution.

4.1.3 Effect of Refractory Period on the p.d.f. of Poisson Process.

The neuronal membrane is refractory immediately after an action potential due to the absolute refractory period, so that the firing probability at the post-membrane depends not only on the stimulus associated with a preceding pulse train but also on the local properties of the post-membrane when the refractory period of the pre- and post-membrane are not consistent. As in some pathological cases, the refractory periods of pre- and post-membrane may not be consistent due to the change of characteristics of the membranes. When studying the action potential train transmission in the biological neural network, the refractory mechanism was seldom considered. However the refractory period, especially the absolute refractoriness, at the post-membrane of a gap junction which electrically connects individual neurons will greatly affect the IPI of the output pulse train observed at the post-membrane when it is greater than that of the pre-membrane. Therefore it will be of great interest to study the p.d.f. of the output IPI by taking into account the factor of the absolute refractory inconsistency at the post-membrane. This section focuses on a theoretical analysis on how the inconsistent absolute refractory period (for simplicity, it is termed as the absolute refractory period of the post-membrane in the content that follows. It is a relative value comparing to the absolute refractory period of the pre-membrane.) affects the p.d.f. of the output IPI with the assumption that the input pulse train at the pre-membrane is a homogeneous Poisson Process.

The input at the pre-membrane, which serves as the stimulus to the post-membrane was simulated as a homogeneous Poisson Process with the exponential IPI distribution given by

$$p(\tau_i) = \lambda_0 e^{-\lambda_0 \tau_i}, \tau_i > 0, \tag{4.5}$$

where λ_0 is the mean firing rate and τ_i is IPI. Since the input pulse train is homogeneously Poisson, the IPIs are independent and have the same p.d.f. as that given in Eq. 4.5. If an input IPI,τ_i, is less than the absolute refractory period, μ, the IPI observed at the output will be $\tau_i + \tau_{i+1}$. If $\tau_i + \tau_{i+1}$ is still less than μ, then the output IPI will be increased by adding the following input IPIs until the summation exceeds the absolute period, μ. The p.d.f. for the sum of several independent random variables will be the convolution between them.

It can be proved as the following. Given $t_2 = \tau_1 + \tau_2$

and

$$p(\tau_1) = p(\tau_2) = \begin{cases} \lambda_0 e^{-\lambda_0 \tau_i} & \tau_i \geq 0 \\ 0 & \tau_i < 0 \end{cases}$$

so we have

$$\begin{aligned} p(t_2) &= p(\tau_1) * p(\tau_2) \\ &= \int_0^{t_2} (\lambda_0 e^{-\lambda_0 \tau_1})[\lambda_0 e^{-\lambda_0 (t_2 - \tau_1)}] d\tau_1 \\ &= \lambda_0^2 e^{-\lambda_0 t_2} \int_0^{t_2} d\tau_1 \\ &= \begin{cases} \lambda_0^2 t_2 e^{-\lambda_0 t_2} & t_2 \geq 0 \\ 0 & t_2 < 0 \end{cases} \end{aligned} \tag{4.6}$$

Assume that

$$p(t_{n-1}) = \begin{cases} \frac{(\lambda_0 t_{n-1})^{n-2}}{(n-2)!} \lambda_0 e^{\lambda_0 t_{n-1}} & t_{n-1} \geq 0 \\ 0 & t_{n-1} < 0 \end{cases}$$

$$p(\tau_n) = \begin{cases} \lambda_0 e^{-\lambda_0 \tau_n} & \tau_n \geq 0 \\ 0 & \tau_n < 0 \end{cases}$$

Since $t_n = t_{n-1} + \tau_n$, we have

$$\begin{aligned} p(t_n) &= p(t_{n-1}) * p(\tau_n) \\ &= \int_0^{t_n} [\frac{(\lambda_0 t_{n-1})^{n-2}}{(n-2)!} \lambda_0 e^{-\lambda_0 t_{n-1}}][\lambda_0 e^{-\lambda_0 (t_n - t_{n-1})}] dt_{n-1} \\ &= \frac{\lambda_0^n}{(n-2)!} e^{-\lambda_0 t_n} \int_0^{t_n} (t_n)^{n-2} dt_{n-1} \\ &= \begin{cases} \frac{\lambda_0^n t_n^{n-1}}{(n-1)!} e^{-\lambda_0 t_n} & t_n \geq 0 \\ 0 & t_n < 0 \end{cases} \end{aligned} \tag{4.7}$$

Therefore, the p.d.f. of the sum of n subsequential IPIs will be

$$\begin{aligned} p_n(\tau) &= p(\tau_1) * p(\tau_2) * ... p(\tau_n) \\ &= \frac{\lambda_0^n \tau^{n-1}}{(n-1)!} e^{-\lambda_0 \tau}, \end{aligned} \tag{4.8}$$

where $\tau = \tau_1 + \tau_2 + ... + \tau_n$.

According to the p.d.f. given in Eq. 4.8, the probability of the IPI greater than the absolute refractory period, μ, is

$$\begin{aligned} P \quad (\quad & \mu \leq \xi < \tau) \\ = \quad & P_1(\mu \leq \xi < \tau) + P_1(0 \leq \xi < \mu) P_2(\mu \leq \xi < \tau) \\ + \quad & ... + P_n(\mu \leq \xi < \tau) \prod_{i=1}^{n-1} P_i(0 \leq \xi < \mu), \end{aligned} \tag{4.9}$$

where $P_n(\mu \leq \xi < \tau) = \int_\mu^\tau p_n(\xi) d\xi$. The last term in Eq. 4.9 is zero when $n \longrightarrow \infty$. It can be proved as follows:

according to Equ. 4.8, the probability of the sum of n input IPIs less than the absolute refractory period, μ, is:

$$\begin{aligned} P_n(0 \leq \xi < \mu) &= \int_0^\mu \frac{(\lambda_0 \xi)^{n-1}}{(n-1)!} e^{-\lambda_0 \xi} d\xi \\ &= \frac{1}{(n-1)!} \int_0^{\lambda_0 \mu} (\lambda_0 \xi)^{n-1} e^{-\lambda_0 \xi} d\lambda_0 \xi \end{aligned}$$

let $\lambda_0 \xi = x$ we have

$$
\begin{aligned}
&= \frac{1}{(n-1)!}\int_0^{\lambda_0\mu} x^{(n-1)}e^{-x}dx \\
&= \frac{1}{(n-1)!}\int_0^{\lambda_0\mu} (-1)x^{(n-1)}de^{-x} \\
&= \frac{-1}{(n-1)!}(\lambda_0\mu)^{n-1}e^{-\lambda_0\mu} - \frac{-1}{(n-2)!}\int_0^{\lambda_0\mu} e^{-x}x^{n-2}dx \\
&= \frac{-1}{(n-1)!}(\lambda_0\mu)^{n-1}e^{-\lambda_0\mu} - \frac{(-1)^2}{(n-2)!}(\lambda_0\mu)^{n-2}e^{-\lambda_0\mu} \\
&+ \frac{(-1)^2}{(n-3)!}\int_0^{\lambda_0\mu} e^{-x}x^{n-3}dx \\
&\cdot \\
&\cdot \\
&\cdot \\
&= 1 - \sum_{i=1}^{n}\frac{1}{(n-i)!}(\lambda_0\mu)^{n-i}e^{-\lambda_0\mu} \\
&= 1 - e^{-\lambda_0\mu}\sum_{i=1}^{n}\frac{(\lambda_0\mu)^{n-i}}{(n-i)!} \qquad (4.10)
\end{aligned}
$$

Since when $n \longrightarrow \infty$, series $\sum_{i=1}^{n}\frac{\lambda_0\mu)^{n-i}}{(n-i)!}$ will converge at $e^{\lambda_0\mu}$. The result in Equ. 4.10 will be zero when n approaching to ∞. Therefore, when n approaching to ∞, the probability,

$$
\begin{aligned}
P(\mu \le \xi < \tau) &= 1 - P_n(0 \le \xi < \mu) \\
&= 1. \qquad (4.11)
\end{aligned}
$$

After differentiating the probability function in Equ. 4.9 with respect to τ, we may obtain the p.d.f. of the output IPIs as follows[71],

$$
p(\tau) = p_1(\tau \ge \mu) + \sum_{k=1}^{n} p_k(\tau \ge \mu)\prod_{j=1}^{k}(1 - e^{-\lambda_0\mu}\sum_{i=0}^{j-1}\frac{(\lambda_0\mu)^i}{i!}). \qquad (4.12)
$$

According to Equ. 4.11, the integration of $p(\tau)$ in Equ. 4.12 is equal to 1 when n approaching to ∞.

Equ. 4.12 reveals the relationship between the absolute refractory period at the post-membrane and the distribution of the firing statistics of the output

action potential train. Fig. 4.4 shows the numerical calculation results of $p(\tau)$ when $\lambda_0 = 20pps$ and the absolute refractory period of the post-membrane is equal to $0ms$ and $20ms$ respectively. When the absolute refractory period is not very large, say less than $20ms$, the value for n is equal to 10 in Equ. 4.12 in the numerical calculation, and the truncated error that induced by the numerical calculation is less than 1% when $\mu = 20ms$. The numerical integration of the two output p.d.f in Fig. 4.4 are 0.999543 and 0.996733 respectively given the integration interval is from $0s$ to $4s$.

Fig. 4.5 shows the comparison between the probabilities of the output IPIs calculated by theoretical formula given in Equ. 4.12 and by simulation when μ is equal to $5, 10, 15ms$ and the input IPIs are Poisson distributed with meanfiring rate $20pps$. From Equ. 4.12, The probability for different IPIs, τ, in a output action potential train are approximated by the product of $p(\tau)$ and $d\tau$ at discrete values of τ, and $d\tau$ is selected small enough in the numerical calculation. The calculated results for the theoretical probabilities are given in solid lines in Fig. 4.5. The circles in Fig. 4.5 represent the statistical probabilities at different values of output IPIs obtained by simulations. Given the value of μ and the input action potential train with 1000 Poisson distributed IPIs and meanfiring rate equal to $20pps$, the output action potential train can be generated by erasing the action potentials which is falling into the absolute refractory period of the post-membrane. By calculating the frequency of different IPIs appearing in the output action potential train, the histogram of the output IPIs can be obtained. If divided the frequencies of each τ by the total sized of output IPIs, then the statistical probability of different τs will be obtained. The results in Fig 4.5 suggest that the probabilities of output IPIs obtained by the theoretical formula and simulation are basicly consistent.

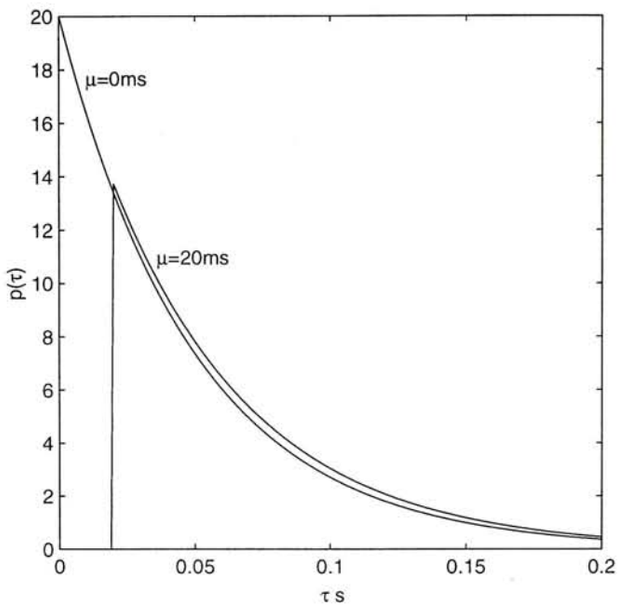

Figure 4.4: The theoretical calculation results of the p.d.f, $p(\tau)$, when $\lambda_0 = 20pps$ and the absolute refractory period of the post-membrane,μ, is equal to $0ms$ and $20ms$.

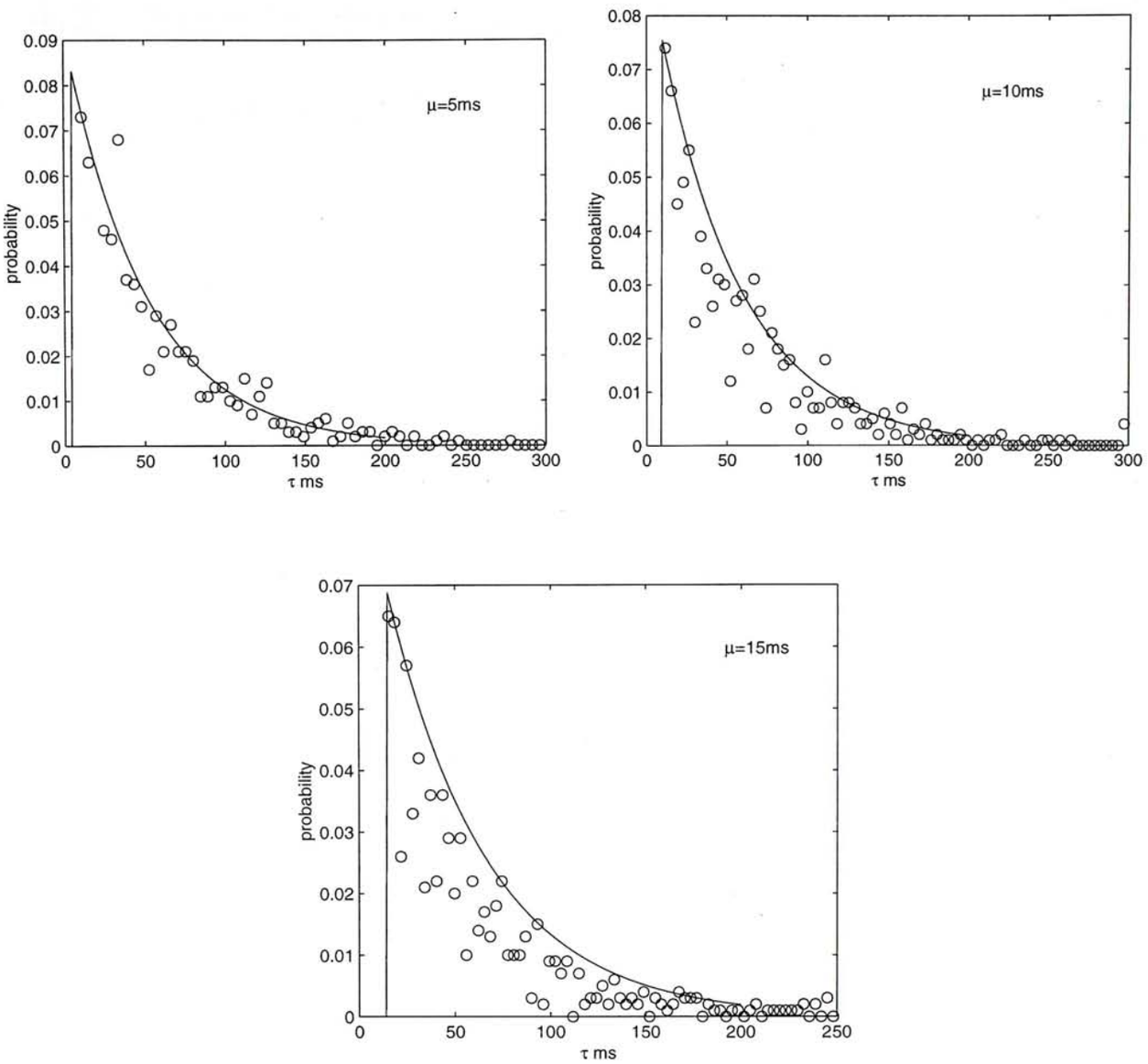

Figure 4.5: Comparison between the theoretical probabilities, the solid lines, and the statistical probabilities, the circles, of simulation of the output IPIs, given $\mu = 5, 10, 15ms$ respectively.

4.2 Simulation of the Action Potential Train Transmission

In the previous section, point process methods are employed in the study of the action potential train transmission. However, as the name for Point Process, the individual action potentials in the train have been simplified to "points", the identical δ functions. The detailed changes in the shape of action potentials are neglected. As indicated in Chapter 2 and Chapter 3, the junctional elements in our model, C_j and R_j, will affect the action potential transmission at the gap junction. The peak delay, peak attenuation and the increased duration are observed at the post-potential. Will these changes affect the action potential train transmission? This question is hard to be answered by Point Process study only. Then the simulation of the action potential train transmission is carried out in our work but surely will be included into our future study.

Although Poisson Process is a widely used assumption for the action potential train[72][73], there are other kind of distributions may be detected in the reality. Examples of some canonical interpulse interval histograms are shown in Fig. 4.6[12]. If a particular firing train is precisely regular, all the IPI will have the same value. The histogram for this case will consist of a single very large peak at the particular time value. This is illustrated in Fig. 4.6.a. This particular pattern is called a pacemaker. If one introduces a certain amount of irregularity into such a train by supposing that the intervals occur with a given mean value, but that the actual individual intervals may be slightly less or greater than this value with, say, a Gaussian distribution, one gets an IPI histogram which approaches a Gaussian distribution as illustrated in Fig. 4.6.b. such a process may be considered a noisy pacemaker. Fig. 4.6.c. shows the Poisson distribution which has

been studied in the previous section. Fig. 4.6.d. is a distribution obtained by truncating a Poisson distribution, which is usually to approximate the effect of the refractory period of the membrane. A similar and related distribution is the gamma distribution shown in Fig. 4.6.e which is described as Equ. 4.13

$$p(\tau) = \frac{a^r \tau^{(r-1)} e^{-a\tau}}{(r-1)!} \tag{4.13}$$

Neuronal firing patterns are often characterized and classified according to how their interval histograms compare to these basic canonical forms. Gaussian and Poisson distributed IPIs are the most commonly encountered cases in neurophysiological study.

Therefore, in our simulation work, the action potential trains with Poisson and Gaussian distributed IPIs are chosen as the inputs to the gap junction model. Fig. 4.7 shows the typical action potential trains occurred at the pre-membrane with (a) Poisson distributed IPI and (b) Gaussian distributed IPI, and each of them contains 100 action potentials. Fig. 4.8 and Fig. 4.9 give the histograms of IPI, τ, for the two action potential trains. In this simulation work, the effects from the model parameter, C_j, on the action potential train transmission are first studied when the input action potential train has the Gaussian distributed IPIs. Then the effects of the refractory period of the post-membrane on the action potential train transmission are analyzed given the input IPIs have the Gaussian and Poisson distribution.

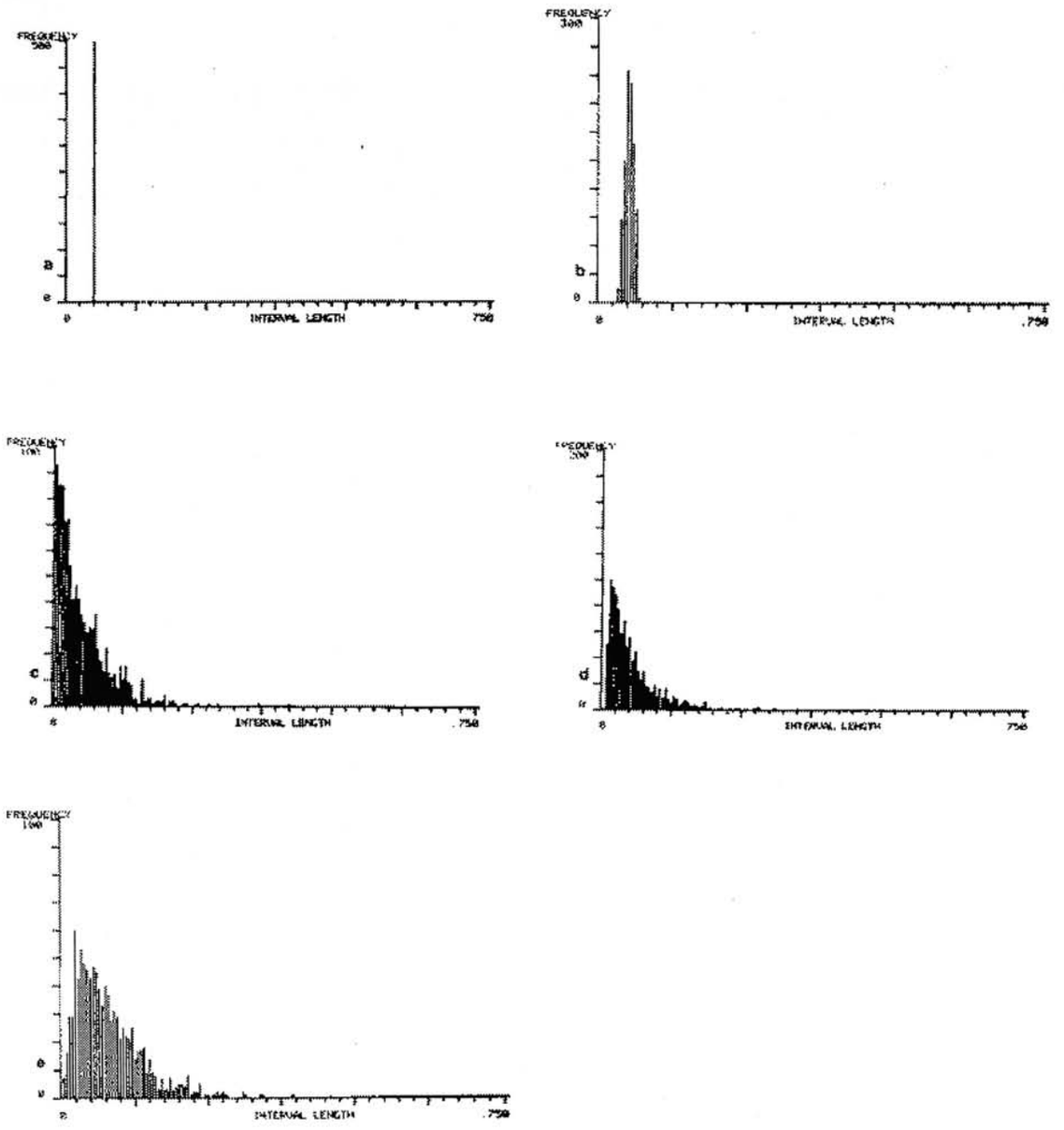

Figure 4.6: First-order interval histograms for several common processes. a. Pacemaker process; b. Noisy pacemaker process; c. Poisson process; d. Truncated Poisson process; e. Gamma process (r=2,a=25).

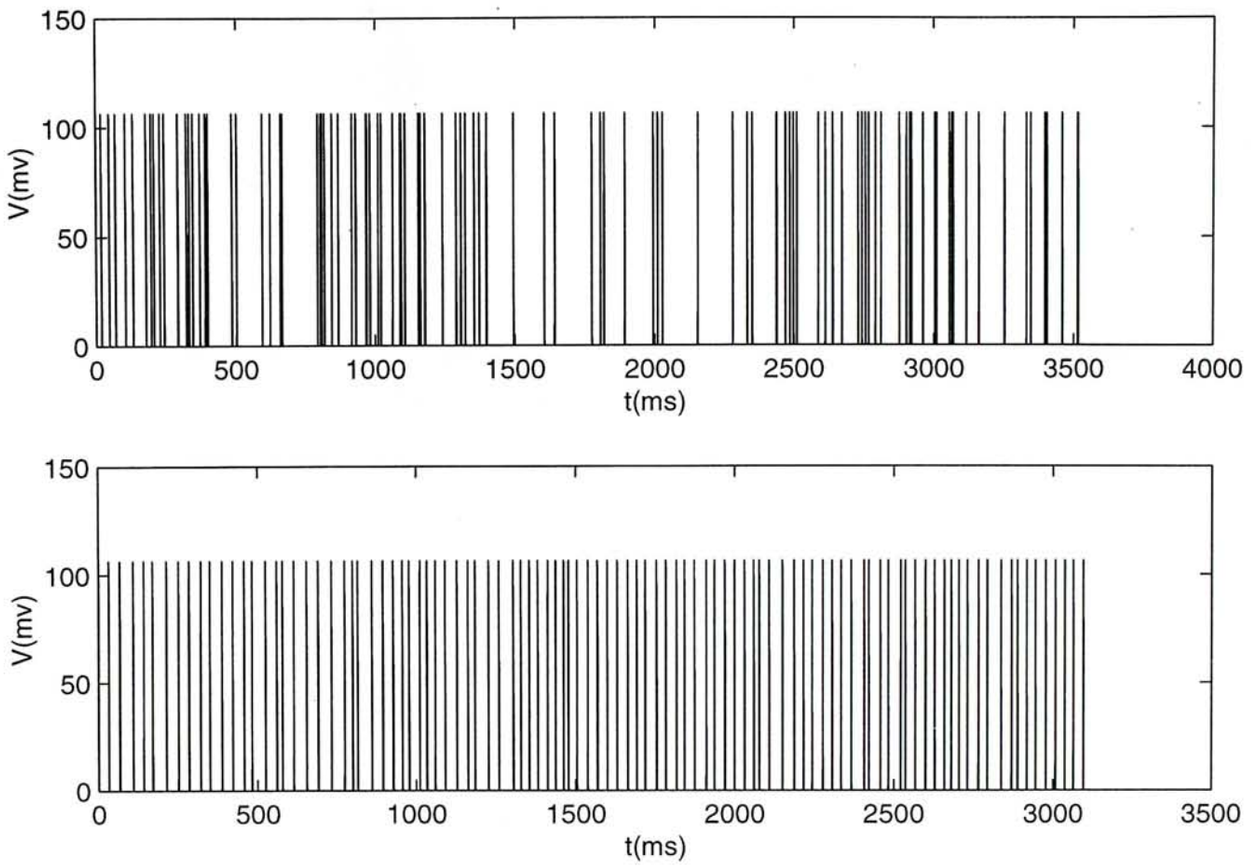

Figure 4.7: Two typical input action potential trains with (a) Poisson distributed IPI when $\lambda = 30pps$ and (b) Gaussian distributed IPI when $\mu = 30ms$ and $\sigma^2 = 50ms^2$.

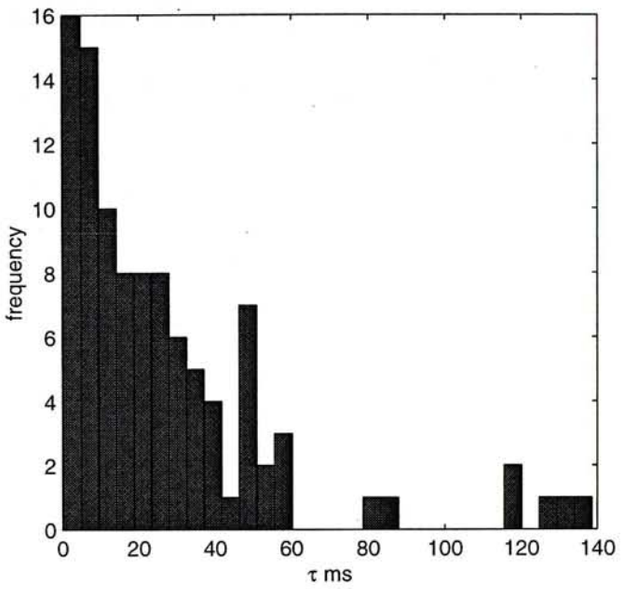

Figure 4.8: The histogram of Poisson distributed IPI.

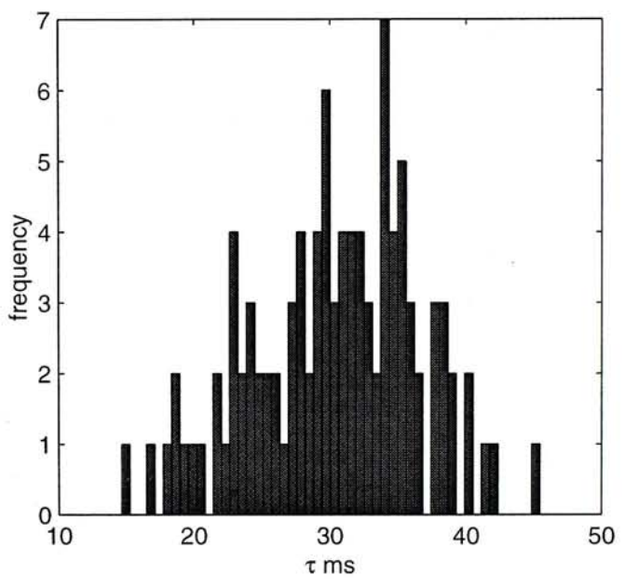

Figure 4.9: The histogram of Gaussian distributed IPI.

4.2.1 Effects of the Model Parameter on the Action Potential Train Transmission

According to the model analysis in Chapter 3, the junctional capacitor, C_j, will cause the peak delay, peak attenuation and the duration change at the post-potential, while R_j only induced the peak delay and the peak attenuation. Thus C_j is selected as the changeable parameter for the simulation study. In order to see how the gap junction parameters or the IPI distribution of the input action potential train affects the action potential train transmission, the refractory period at the post-membrane is not considered temporally. It also means that we consider that the refractory period of the pre- and post-membrane are the same and the action potentials that generated at the pre-membrane will not be erased by at the post-membrane due the refractoriness.

Methodology

Since in the Poisson precess the most likely IPI in the action potential train is $\tau = 0$ as it is shown in Fig. 4.8. However, it is not the case in the reality due to the absolute refractoriness of the membrane. Thus Poisson process is not studied in this part but only the Gaussian distributed IPI. As the mechanism of refractory period has not been taken into account, we first assume that the IPI of the pulse train at the input is large enough to avoid overlapping of the action potentials occurring at the pre- or post-membrane. The IPI with Gaussian distribution is adopted with the mean value equal to 30ms and the largest variance equal to 50 ms^2. Furthermore we assume that in one action potential train the individual action potentials have the same amplitude and same pulse duration. The action potential train given as the input at the pre-membrane is fixed at an fixed observation time interval of 1000ms, although the action potential train is less than 1000ms, with the given number of 20 pulses. Each pulse in the train

will evoke only one action potential at the post-membrane. Since signals can not only be represented in the time domain but also in the frequency domain. For random processes, the power density spectral (PDS) is a common method to analyze signals. The computation of the output PDS is carried out by the numerical method with Matlab. The sampling frequency is about 15 times of the highest frequency of the single action potential. The average frequency of the output pulse train is evaluated by the moment method as given in Equ. 4.14,

$$\bar{f} = \frac{\int_0^\infty f \cdot S_y(f)df}{\int_0^\infty S_y(f)df} = \frac{M_1}{M_0}, \tag{4.14}$$

where the $S_y(f)$ is the PDS of the output at the post-membrane side, and M_1 and M_0 are the first and the zero moments respectively. While the integration interval in frequency domain is set from 0 to 1000Hz, beyond which the amplitude of PDS of the output is almost zero everywhere.

Simulation Results

Fig. 4.10 gives the results of the calculated single action potential with C_j=2μF/cm^2, a typical action potential train at the post-membrane side, and their corresponding power density spectra, with the variance σ^2 of the IPI equal to $1ms^2$.

Fig. 4.11 shows the output pulse train in time domain and its PDS with the variance σ^2 of IPI equal to $50ms^2$ (other parameters are the same as those of Fig. 4.10). Fig. 4.12 gives the linear regression result of the average frequency $\bar{f}$ and variance σ^2 over 11 pairs of data. Fig. 4.13 gives the linear regression result of the calculated values of $E[S_y(\lambda)/S_y(0)]$ versus the change of the IPI variance σ^2. Fig. 4.14 illustrates the effects of C_j on average frequency $\bar{f}$.

Comparing the power spectral densities of pulse trains at different values of IPI variance in Fig. 4.10 and Fig. 4.11, one may find that the PDS of the synaptic output becomes discrete when the IPI variance is small. The power of DC in the PDS and the mean firing rate λ are all the same (2.7581W/Hz for DC power and

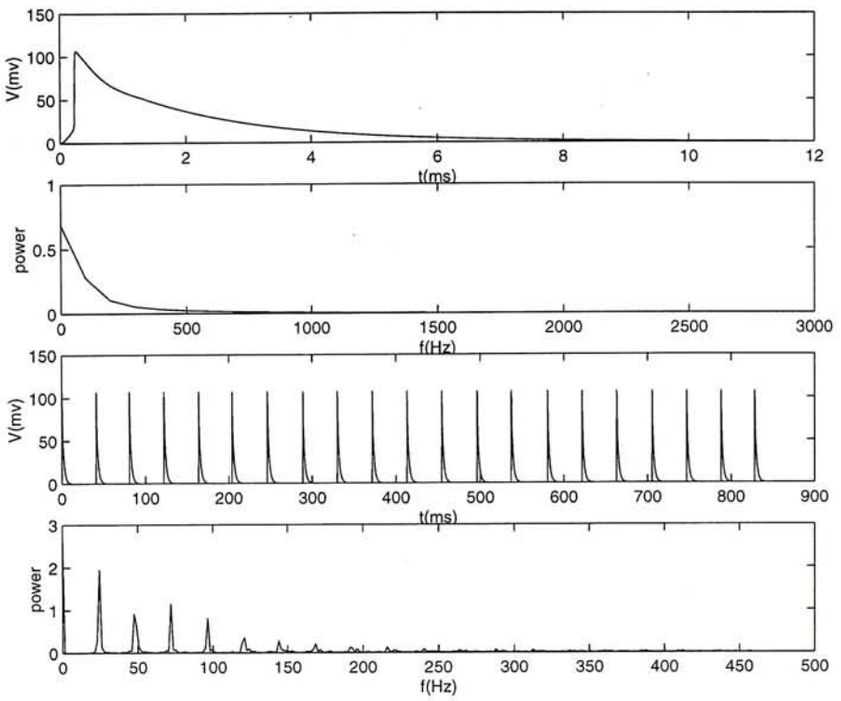

Figure 4.10: a) The single action potential of the post-membrane with C_j equal to $2\mu\text{F}/cm^2$ in the time domain; b) The PDS of the single action potential; c) The action potential train with the variance equal to $1ms^2$ obtained at the post-membrane; d) The PDS of the action potential train.

24.5Hz for mean firing rate 24.5pps) for the two trains. It is observed that the power at the higher frequencies decreases when the variance increased. As shown in Fig. 4.12, the average frequency $\bar{f}$ decreases by 1% with the increase of the variance. It may suggest that the change of the variance would not affect the average frequency. However, when given a small variance, the average frequency will decrease with the increase of the mean firing rate. It is because with small variance the action potential train may be regarded almost periodic. For periodic action potential train, the PDS is discrete and may be considered as the sampling of the PDS of single action potential in the frequency domain. Then the larger the meanfiring rate the lager the space between the neighboring bins in the frequency domain. Therefore it is easy to imagine when increasing the mean firing rate of the action potential train the more energy will concentrate on the lower frequency

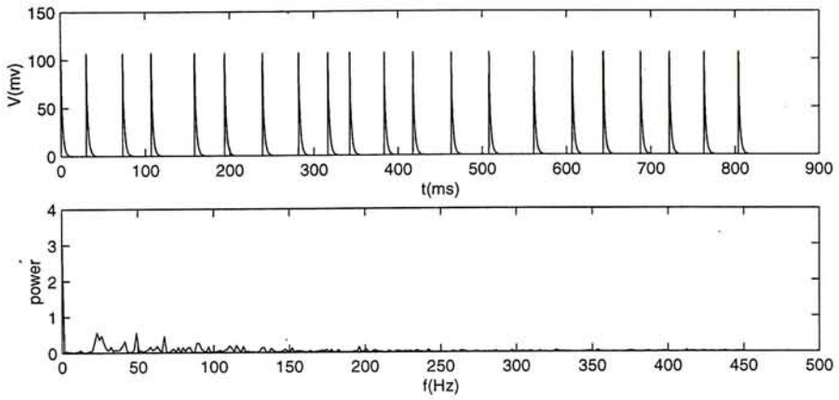

Figure 4.11: The pulse train in time domain and its PDS with σ^2 equal to 50 ms^2 and C_j equal to $2\mu\text{F}/cm^2$, the mean firing rate λ at 24.5pps.

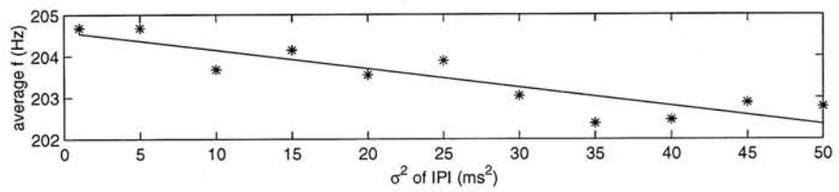

Figure 4.12: The relationship between the average frequency $\bar{f}$ and variance σ^2, given C_j equal to $2\mu\text{F}/cm^2$ and mean firing rate λ at 24.5pps.

in the PDS. Therefore the average frequency decrease with the increasing of the mean firing rate. The amount of change in average frequency also depends on the single action potential and the firing statistics of the pulse train. If using the ratio of the power at DC to the power at the mean firing frequency λ as a measure, the influence of the variance in IPI will be seen clearly. The result of linear regression in Fig. 4.13 shows a decrease of the $E[S_y(\lambda)/S_y(0)]$ with increasing the variance of IPI. The peak attenuation and the peak delay can be explained in the frequency domain by the low pass characteristic of the electrical synapse. With larger values of the capacitance C_j, the synapse exhibits lower pass characteristics, as a result, the average frequency $\bar{f}$ reducing to the lower end. It is shown in Fig. 4.14 that when C_j is increased from $4\mu\text{F}/cm^2$ to $24\mu\text{F}/cm^2$, the range is within that selected in Chapter 2 for physiological meaning, the average frequency $\bar{f}$ of the output pulse train almost decreases to its 66.7%, much more than that caused by

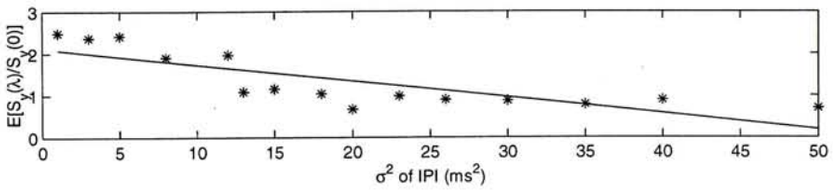

Figure 4.13: The relationship between the variance σ^2 of IPI and $E[S_y(\lambda)/S_y(0)]$, given C_j equal to $2\mu F/cm^2$ and mean firing rate λ at 24.5pps.

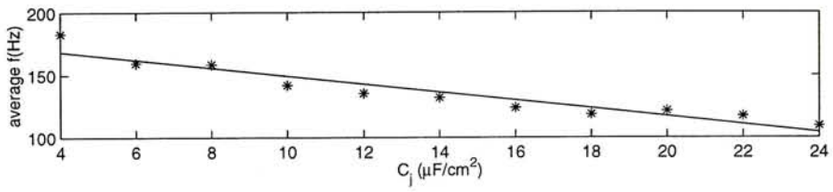

Figure 4.14: The relationship between the average frequency $\bar{f}$ and C_j, given variance σ^2 equal to $1ms^2$ and mean firing rate λ at 24.5pps.

changes in the variance of IPI.

4.2.2 Effects of the Refractory Period of the Post-membrane on the Action Potential Train Transmission

As discussed previously, the junctional parameters C_j and R_j will affect the average frequency due to the consequent peak attenuation and peak delay of the individual action potential transmission, but they do not affect the number of the action potentials at the post-membrane. Therefore the incoming pulse train at the pre-membrane may have the same firing statistical behavior as that of the pulse train at the post-membrane, if the refractory period is not considered in the model. The output mean firing rate detected at the post-membrane can be changed, if considering the mechanism of the absolute refractory period[75]. The simulation of the action potential train at the pre-membrane is conducted by an assigned IPI distribution. In this study two distributions were adopted. One is an exponential distribution with the assumption that the incoming pulse train is

a homogeneous Poisson Process, as given by,

$$p(\tau) = \lambda_0 e^{-\lambda_0 \tau}, \tau > 0, \tag{4.15}$$

where λ_0 is the mean firing rate of the input pulse train and τ is the IPI. In the simulation, λ_0 is set at the value of $20pps$. In reality, the exponential distributed IPI is impossible in the excitable cells since the membrane will be inactive due to the refractory period as has been discussed in the last section. Thus the probability of the IPI equal to zero should be zero in reality. Instead of the exponentially distributed IPIs of the pulse train, a normal distribution most likely occurs in practice. Therefore in order to make a comparison with the widely used Poisson Process a normal IPI distribution of the incoming train with the mean value of $50ms$ ($\lambda_0 = 20pps$) was also chosen in this work,

$$p(\tau) = \frac{1}{\sigma\sqrt{2\pi}} e^{\frac{-(x-50)^2}{2\sigma^2}}, \tag{4.16}$$

where the standard deviation, σ, is set at 10ms in the simulation in order to achieve the high probability of the IPIs large than zero. To make the simulation results comparable, the meanfiring rate for the two distributions are set to be equal, i.e., $\lambda_0 = 20pps$. In the calculation, the pulse train generated at the pre-membrane contains 100 action potentials. Fig. 4.15 shows a simulated sample for the action potential train generated at the pre-membrane and the pulse train obtained at the post-membrane.

If the pulses from the pre-membrane fall in the absolute refractory period of the post-membrane, they will be "erased" in the output action potential train.The range of the variation in the absolute refractory period, μ, was selected from $0ms$ to $50ms$. The mean firing rate of the output was estimated by the averaged number of the action potentials over the time duration of the whole pulse train.

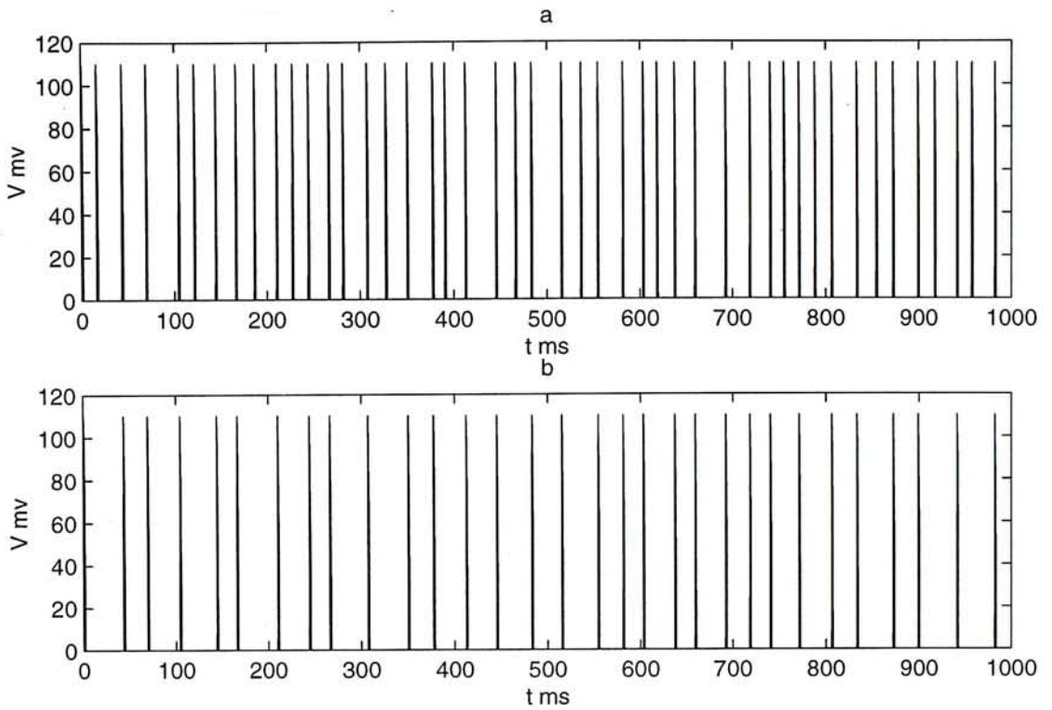

Figure 4.15: (a)The simulated input action potential train generated at the pre-membrane, and (b)the simulation result of the output action potential train obtained at the post-membrane, with the exponential input IPI distribution and the refractory period $\mu = 10ms$.

4.3 Results

Fig. 4.16 shows the relationship between the output mean firing rate and the absolute refractory period for the input IPIs with the exponential distribution. It is clear that the output mean firing rate decreases when the refractory period of the post-membrane increases. Fig. 4.17 shows the relationship between the output mean firing rate and the absolute refractory period for the input IPIs with the Gaussian distribution. For the input IPI with the Gaussian distribution, the output mean firing rates do not change greatly for μ ranging from $0ms$ to $30ms$. When μ is larger than $30ms$, the output mean firing rate at the post-membrane decreases.

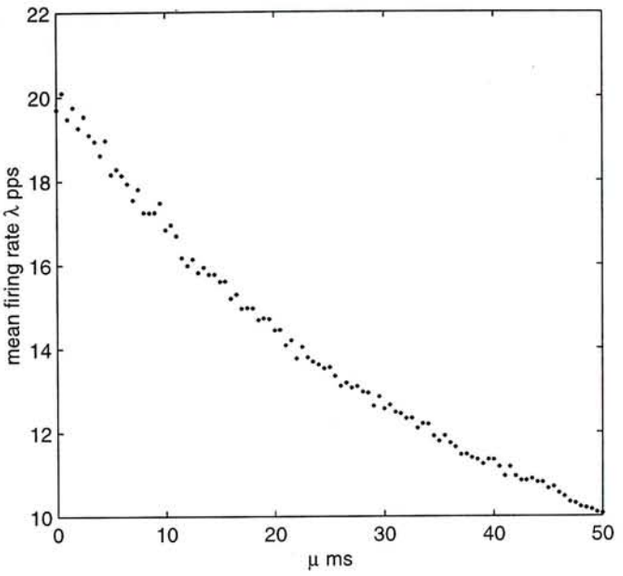

Figure 4.16: The relationship between the output mean firing rate and the absolute refractory period for the input exponential IPI distribution with $\lambda_0 = 20pps$.

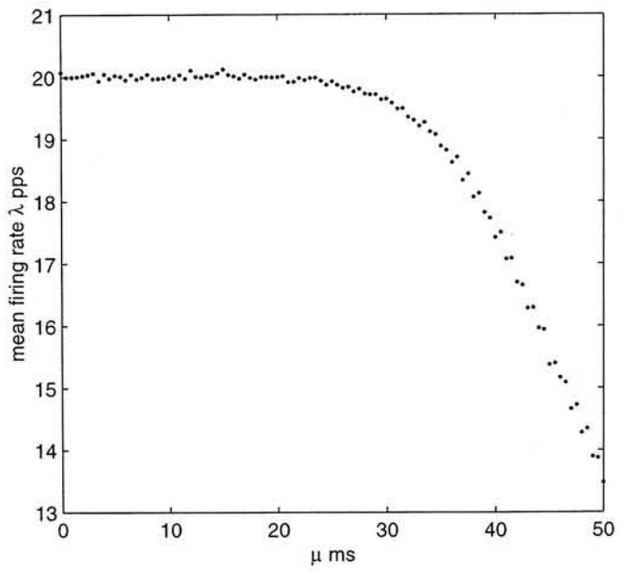

Figure 4.17: The relationship between the output mean firing rate and the absolute refractory period for the Gaussian input IPI distribution with $\mu_\tau = 50ms$ and $\sigma = 10ms$.

4.3.1 Section Summary

According to the obtained results in the study of model parameter, it can be concluded that the synapse has the strong low pass property which can be illustrated by the obvious reducing of the average frequency to the lower region in the output PDS. Traditionally, the peak attenuation and peak delay are applied as the measure of the output at the post-membrane to analyze the synaptic properties. However, they would not be enough for understanding the whole physiological properties of the synapse. The peak delay and the duration change of the post-potential are reflected as the whole low pass characteristic in the PDS of the output, and the peak attenuation of the individual action potential at the post-membrane appears as the decreased power at the DC. It will be of great value if the characteristics of the peak delay and the duration increase in the frequency domain may be picked up individually in the obtained PDS. The low pass characteristic of the synapse also suggests that the individual action potential shape should not be ignored when studying the detailed features of the nerve system, unlike the study of neuron signaling where the individual action potential can be simplified as the δ function.

The results on the relationship between the output mean firing rate and the absolute refractory period show that the selection of the p.d.f. of the input IPIs greatly affect the mean firing rate of the output for the certain values of the absolute refractory. With exponential input IPI distribution, the output mean firing rate at the post-membrane is very sensitive to the change of the absolute refractory period of the membrane. With the Gaussian distributed IPIs, the output mean firing rates are almost same as that of the input when the absolute refractory μ is a half of the input mean IPI ($25ms$). The results would be useful in the design of electrical neuro-muscular stimulators.

Chapter 5

Conclusions and Future Studies

5.1 Conclusions of Major Contributions

- **Model Development:** Based on the Frankenhaeuser-Huxley (F-H) equation, a new circuitry model of rectifying electrical synapse is developed for understanding the behavior at the rectifying gap junction or giant motor synapse of crayfish[52]. It can be concluded from the results of the simulation that the new circuitry model can reconstruct the peak delay, peak attenuation and the duration changes only by adjusting the junctional parameters, i.e., C_j and R_j. Due to its simplicity, the gap junction model is easy to be incooperated into other circuitry models for gap junctionally coupled models in neural network modeling.

- **Theoretical Analysis of the Model:** The results of the model analysis also show that the increased capacitance at the gap junction may be one of the reasons in the understanding of some pathological cases like aschimia in the heart. The time constant is an important measure at the gap junction. The duration change of the post-potential can be quantified by calculating

the time constant at the gap junction[57]. It is also proved in Chapter.2 that the new element, C_j, at the gap junction can not be ignored in the explanation of the duration change at the post-potential. In the second part of the theoretical analysis of the model, it is indicated that the steady state voltage defendant conductance of Giaume's kinetic model can be reconstructed by our circuitry model given the same parameter ranges as that for Giaume's model.

- **A Study on the Effects of Refractory Period on the Action Potential Train Transmission:** The concepts and the methods of Point Process are employed in the study of theoretical analysis of the inconsistent refractory period of the post-membrane when given the input at the pre-membrane of the gap junction is action potential train with Poisson distributed IPIs[71]. The p.d.f. of the output action potential train is obtained after taking into account of the factor, the refractory period. A Simulation study is carried out in order to investigate the effects of the model parameter on the action potential train transmission[74] and to study how the inconsistency of the refractory period of the post-membrane affects the transmission characteristics when the input action potential train has different distributed IPIs[75]. The results of this chapter suggest that the refractory period will greatly affect the output p.d.f. and meanfiring rate. The analysis may provid some suggestions for the design of electrical stimulators.

5.2 Topics for Future Studies

The development of the rectifying electrical synapse model is only a start point in the study of the whole neural network and the gap junctionally coupled cell-networks. The purpose of the modeling is trying to understand the intact function of the biological systems. Therefore, our work will not stop here but will carry on towards the aim stated above. The following is a list of possible topics for the future endeavors in the cell-network studies.

- **Extension of the Model:** The study on the two dimensional electrophysiologic models of heart cells and cell-network done by Torres etc. only considered the pure resistive connection between the cells[24]. The new model developed in our work may be applied to the two dimensional or even three dimensional cell-network to simulate the real physiological phenomena. Firstly it can be investigated whether it will provide more new information than the results given by Torres. Secondly, we will try to relate the network model to the pathological cases and to find out whether it can proved any useful suggestions for diagnosis.

- **Signal Processing Characteristics Study:** After the development of the cells network connected by gap junction model, the signal processing characteristic study is necessary to be brought out. The firing statistics of the neuron pools may be carried out, especially the study of dispersion of the refractoriness at the post-membranes. The time and frequency analysis over the signals may provide us the better understanding of the function of the cell network being modeled.

- **A Study of the Velocity of the Signal Transmission:** It once has been mentioned in Knisley's work that the junctional parameters will affects the

transmission velocity[76]. But what has been done in that work is stopped at the simulation level, and the model for the gap junction has not been updated. Therefore, it is possible for us to study the relation between the signal transmission velocity and the junctional elements with our circuitry model. Furthermore, the theoretical analysis on that relation may set as another subject for the future work.

Bibliography

[1] Irwin B. Levitan, Leonard K. Kaczmarek, The Neuron, Cell and Molecular Biology, *Oxford University Press, New York* 1991.

[2] M. P. Sheetz, E. R. Steuer, and T. A. Schroer, The Mechanism and regulation of Fast Axonal Transport, *Trends Neurosci.* **12**:474-478, 1989.

[3] L. K. Kaczmarek, M. Finbow, J-P. Revel, and F. Strumwasser, The Morphology and Coupling of Aplysia Bag Cells Within the Abdominal Ganglion and in Cell Culture, *J. Neurobiol.* **10**:525-550, 1979.

[4] S. Jaslove and P. Brink, The Mechanism of Rectification at the Electrotonic Motor Giant Synapse of the Crayfish, *Nature* **232**:63, 1986.

[5] A. A. Auerbach and M. V. L. Bennett, A Rectifying Synapse in the Central nervous System of a Vertebrate, *J. Gen. Physiol.* **53**:211, 1969.

[6] J. E. Saffitz, L. M. Davis, B. J. Darrow, et al, The Molecular Basis of Anisotropy: Role of Gap Junctions, *J. Cardiovasc Electrophysiol.* **6**:498-510, 1969.

[7] H. A. Fozzard, M. F. Arnsdorf, The Heart and Cardiovascular System. *Raven Press Ltd.* **New York**, 1992.

[8] N. J. Sever, Pathophysiology of Gap Junctions in Heart Disease, *J. Cardiovasc Electrophysiol.* **5**:462-475, 1994.

[9] H. L. Kanter, E. C. Beyer, J. E. Saffitz, Structural and Molecular Determinants of Intercellular Coupling in Cardic Myocytes, *Microsc. Res. Tech.* **31**:357-363, 1995.

[10] N. S. Peters, C. R. Green, P. A. Poole-Wilson, et al, Cardiac Arrhythmogenesis and the Gap Junction, *J. Mol Cell Cardiol.* **27**:37-44, 1995.

[11] James W. Holder, E. Elmore and J. C. Barrett, Gap Junction Function and Cancer, *Cancer Research* **53**:3475-3485, Aug 1, 1993.

[12] R. J. Macgregor and E. R. Lewis, Neural Modeling: Electrical Signal Processing in the Nervous System, *Plenum Press New York and London*, 1977.

[13] D. E. Goldman, Potential, Impedance and Rectification in Membranes, *J. Gen. Phys.* **27**:37-60, 1943.

[14] A. L. Hodgkin and A. H. Rushton, The Electrical Contents of a Crustacean Nerve Fibre, *Proc. Royal. Soci(B:bio)* **133**:434-444, 1946.

[15] B. Frankenhaeuser and A. F. Huxley, The Action Potential in the Myelinated nerve fiber of Xenopus Laevis as Computed on the Basis of Voltage Clamp Data, *J. Physiol.* **171**:302-315, 1964.

[16] D. Noble, A Modification of the Hodgkin-Huxley Equations Applicable to Purkinje Fibre Action and Pacemaker Potentials, *J. Physiol.* **250**:1-59, 1975.

[17] R. E. McAllister, D. Noble, R. W. Tsien, Reconstruction of the electrical activity of Cardiac Purkinje Fibres., *J. Physiol.* **160**:317-352, 1962.

[18] D. DiFrancesco and D. Noble, A Model of Cardiac Electrical Activity Incorporating Ionic Pumps and Concentration Changes., *Phil Trans R Soc Lon B* **307**:353-398, 1985.

[19] G. W. Beeler and H. Reuter, Reconstruction of the Action Potential of ventricular Myocardial Fibre, *J. Physiol.* **268**:177-210, 1977.

[20] J. P. Drouhard and F. A. Roberge, A Simulation Study of the Ventricular Myocardial Action Potential, *IEEE Trans Biomed Eng.* **29**:494-502, 1982.

[21] C. H. Luo and Y. Rudy, A Model of the Ventricular Cardiac Action Potentiall Depolarization, Repolarization, and their Interaction., *Circ. Res.,* **68(6)**:1501-1526, 1991.

[22] C. H. Luo and Y. Rudy, A Dynamic Model of the Cardiac Ventricular Action Potential. I. Simulations of Ionic Currents and Concentration Changes, *Circ. Res.,* **74(6)**:1071-96, 1994.

[23] J. Zeng, K. R. Laurita, D. S. Rosenbaum and Y. Rudy, Two components of the Delayed Rectifier K^+ Current in Ventricular Myocytes of the Guinea Pig Type. Theoretical Formulation and Their Role in Repolarization., *Circ. Res.,* **77**:140-152, 1995.

[24] V. Torres, JMJ. Ferrero, M. Monserrat, J. Saiz, J. M. Ferrero, N. V. Thakor, Simulation Study of Epicardial Action Potential Under Normal and Ischemic Conditions., *Computers in Cardiology* **Indianapolis**:165-169, 1997.

[25] C. Nordin, Computer Model of Membrane Current and Intracellular Ca^{2+} flux in the isolated guinea pig ventricular myocyte., *Am J Physiol,* **265**:H2117-H2136, 1993.

[26] S. S. Demir, J. W. Clark, C. R. Murphy, W. R. Gilles, A Mathematical Model of the Rabbit Sinoatrial Node Cell, *Am J. Physiol.,* **266**:H932-H852, 1994.

[27] D. S. Lindblad, C. R. Murphey, J. W. Clark, W. R. Giles, A Model of the Action Potential and Underlying Currents in a Rabbit Atrial Cell., *Am J. Physiol.,* **271**:H1666-H1696, 1996.

[28] E. J. Furshpan, D. D. Potter, Transmission at the Giant Motor Sy napses of the Crayfish, *J. Physiol.,* **145**:289-325, 1959.

[29] W. C. Cole, J. B. Plcone, N. Sperelakis, Gap Junction Uncoupling and Discontinuous Propagation in the Heart: a Comparison of Experimental Data with Computer Simulations, *Biophys. J,* **53**:809-818, 1988.

[30] L. A. Cartee, R. Plonsey, The Effect of Cellular Discontinuities on the Transient Subthreshold Response of a One-Dimensional Cardiac Model, *IEEE Trans. on BME,* **39**:260-270, 1992.

[31] N. V. Thakor, Electrophysiologic Models of heart Cells and Cell Networks, *EMB Magazine,* **17**:73-83, 1998.

[32] M. V. L. Bennett, Physiology of Electrotonic Junctions, *Ann. N. Y. Acad. Sci.,* **137**:509-539, 1966.

[33] E. C. Fear, M. A. Stuchly, A novel Equivalent Circuit Model for Gap-connected Cells, *Phys. Med. Biol.,* **43**:1439-1448, 1998.

[34] C. Giaume, R. T. kado, H. Korn, Voltage Clamp Analysis of a Crayfish Rectifying Synapse, *J. Physiol.,* **386**:91-112, 1987.

[35] P. R. Gray, Conditional Probability Analyses of the Spike Activity of Single neurons, *Biophys. J.,* **7**:759-777, 1967.

[36] R. P. Gaumond, D. D. Kim, Stimulus and Recovery Dependence of Cat Cochlear Nerve Fiber Spike DisCharge-history Effects, *J. Acoust. Soc. Am.,* **48**:856-873, 1982.

[37] D. H. Johnson, A. Swami, The Transmission of Signals by Auditory Nerve Fiber Discharge Patterns, *J. Acoust. Soc. Am.,* **74**:493-501, 1983.

[38] M. I. Miller, Algorithms for Removing Recovery-related distortion from Auditory Nerve Discharge Patterns, *J. Acoust. Soc. Am.,* **77**:1452-1464, 1985.

[39] M. J. Berry II, M. Meister, Refractoriness and Neural Precision, *J. Neurosci.,* **18(6)**:2200-2211, 1998.

[40] P. A. Getting, Modification of neuron Properties by Electrotonic Synapses. I Input Resistance, Time Constant, and Integration, *J. Neurophysiol.,* **37**:847-857, 1973.

[41] N. M. Kumar, N. B. Gilula, The Gap Junction Communication Channel, *Cell,* **84**:381-388, 1996.

[42] K. S. Cole, H. A. Antosiewicz, P. Rabinowitz, Automatic Computation of Nerve Excitation, *Journal of the Society for Industrial and Applied Mathematics,* **3**:3, 1955.

[43] A. L. Hodgkin, A. F. Huxley, A Quantitative Description of Membrane Current and Its Application to Conduction and Excitation in Nerve, *J. Physiol.,* **117**:500-544, 1952.

[44] J. C. Dalton, R. FitzHugh, Applicability of Hogdkin-Huxley Model to Experimental Data from the Giant Axon of Lobster, *Science,* **131**:1533-1534, 1960.

[45] B. Frankenhaeuser, Delayed Currents in Myelinated Nerve Fibres of Xenopus Laevis Investigated with Voltage Clamp Technique, *J. Physiol.,* **160**:40-45, 1962.

[46] B. Frankenhaeuser, Instantaneous Potassium Currents in Myelinated Nerve Fibre of Xenopus Laevis, *J. Physiol.,* **160**:46-53, 1962.

[47] B. Frankenhaeuser, Potassium Permeability in Myelinated Nerve Fibres of Xenopus Laevis, *J. Physiol.,* **160**:54-61, 1962.

[48] B. Frankenhaeuser, Inactivation of the Sodium-carring Medunism in Myelinated Nerve Fibre of Xenopus Laevis, *J. Physiol.,* **169**:445-451, 1963.

[49] C. Peracchia, Low Resistance junctions in Crayfish. I. Two Arrays of Globules in Junctional Membranes, *J. Cell Biol.,* **57**:54, 1973.

[50] L. Makowski, D. L. D. Caspar, W. C. Phillips, D. A. Goodenough, Gap Junction Structures. II. Analysis of the X-ray Diffraction Data, *J. Cell Biol.,* **74**:629-645, 1977.

[51] S. W. Jaslove, P. R. Brink, The Mechanism of Rectification at the Electrotonic Motor Giant Synapse of the Crayfish, *Nature,* **323**:63, 1986.

[52] X. L. Hu, Y. T. Zhang, J. L. Bao, Modeling of Electrical Synapse: Effects of Model Parameters on the Transmission Characteristics of Electrical Activities, *Proc. of the* 24^{th} *Canadian Medical and Biological Engineering Society Conference, Edmonton, Canada,* 1998.

[53] C. Leclerc, The Roles of Gap Junctions in Early development in Molecular Mechanisms of Epithelial Cell Junctions: From Development to Disease, *S. Citi, ed.(Austin, Texas: R. G. Landes Company),* 45-65, 1994.

[54] W. R. Loewenstein, Junctional Intercellular Communication: the Cell-to-cell Membrane Channel, *Physiol. Rev.,* **61**:829-913, 1981.

[55] D. C. Spray, Physiological and Pharamacological Regulation of gap Junction Channels, in Molecular Mechanisms of Epithelial Cell Junctions, from Development to Disease, *S. citi, ed. (Austin, Texas: R. G. Landes Company),* 195-215, 1994.

[56] D. C. Spray, R. Dermietzed, X-linked dominant Charcot-Mario-Tooth disease and Other Potential Gap Juntion Disease of the Nervous System, *Trends Neurosci.,* **18**:256-262, 1995.

[57] X. L. Hu, Y. T. Zhang, J. L. Bao, Theoretical Analysis of a Rectifying Gap Junction Model, *Proc. of the* 3^{th} *International Workshop on Biosignal Interpretation 99, Chicago, U.S.,* 1999.

[58] a. L. Hodgkin, The Membrane Resistance of a Nonmedullated Nerve Fibre, *J. Physiol.,* **106**:305-318, 1947.

[59] W. C. DeMello, R. Cherry, S. Manivannan, Electrophysiologic and Morphologic Abnormalities in the Failing Heart; Effect of Enalapril on the Electrical Properties, *Cardiac Failure,* **3**:53-62, 1997.

[60] D. C. Spray, R. Dermietzed, X-linked dominant Charcot-Mario-Tooth disease and Other Potential Gap Juntion Disease of the Nervous System, *Trends Neurosci.,* **18**:256-262, 1995.

[61] L. K. Kaczmarek, A Model of Cell Firing Patterns during Epileptic Seizures, *Biol. Cybernet.,* **22**:229-234, 1976.

[62] B. Hille, Ionic Channels of Excitable Membranes, *Sanderland MA: Sinauer Associates,* 1984.

[63] D. H. Perkel, G. L. Gerstein, G. P. Moore, Neuronal Spike Trains and Stochastic Point Processes. I. the Single Spike Train, *Biophysical Journal,* **7(4)**:419:440, 1967.

[64] S. H. Perkel, J. Schulman, T. Bullock, G. Moore, J. Segundo, Pacemaker neurons: Effects of Regularly Spaced Synaptic Input, *Science,* **145**:61:63, 1964.

[65] H. Noda, W. R. Adey, Neuronal Firing in Sleep and Wakefulness, *Brain Research,* **19**:263:275, 1970.

[66] D. M. keenan, J. D. Veldhuis, A Biomathematical Model of Time-delayed Feedback in the Human Male Hypothalamic-pituitary-leydig cell Axis, *American Journal of Physiology,* **275**:E157-76, 1998.

[67] M. Watanabe, K. Aihara, S. Konodo, A Dynamic Neural Network with Temporal Coding and Functional Connectivity, *Biol. Cybenet.,* **78(2)**:87:93, 1998.

[68] S. Nag, Cold-injury of the Cerebral Cortex: Immunolocalization of Cellular Proteins and Blood-brain Barrier Permeability Studies, *J. of Neuropathology & Experimental Neurology,* **55(8)**:880-8, 1996.

[69] A. Eblen-Zajjur, Analysis of Single and Multiple Neuronal Discharges as Point Processes: a Computer Program Set, *Acta Cientifica Venezolana,* **46(1)**:34:40, 1995.

[70] Y. Hamada, Y. Tamai, E. Miyashita, A. Kimura, Evaluation of the Functional Connectivity in the Nervous System Using Time Dependent Scatter Diagrams, *Brain Research,* **660(2)**:209:15, 1994.

[71] X. L. Hu, Y. T. Zhang, J. L. Bao, Effects of the Refractory Period on the IPI Probability Density Function of Junctional Output Pulse Train, *under press, Proc. of* 21^th *Annual International Conference of the IEEE Engineering in Medicine and Biology Society 99,* 1999.

[72] E. Skogvoll, B. H. Lindqvist, Modeling the Occurrence of Cardiac Arrest as a Poisson Process, *Annals of Emergency Medicine,* **33(4)**:409:17, 1999.

[73] R. A. Weale, Lenticular Fluorescence as a Poisson Process, *Investigation Ophthalmology & Visual Science,* **40(1)**:257:60, 1999.

[74] X. L. Hu, Y. T. Zhang, J. L. Bao, A Study of a Recitifying Electrical Synapse Activated with a Random Action Potential Train, *Proc. of* 20^th *Annual International Conference of the IEEE Engineering in Medicine and Biology Society 98, Hong Kong* 1998.

[75] X. L. Hu, Y. T. Zhang, J. L. Bao, Effects of the Refractory Period on Mean Firing Rates at the Gap Junctional Output, *Proc. of* 25^th *the Canadian Medical and Biological Engineering Society Conference, London,* 1999.

[76] S. B. Knisley, W. Krassowska, T. C. Plikington, W. M. Smith, Effect of Intercellular Capacitance on Conduction in a Model of Cell Uncoupling, *Proc. of Annual International Conference of the IEEE Engineering in Medicine and Biology Society,* **12(2)**620-621, 1990.